NAG1601

Six-Axis Monopropellant Propulsion System for Picosatellites

A Major Qualifying Project Report
Submitted to the Faculty
of the
WORCESTER POLYTECHNIC INSTITUTE
in partial fulfillment of the requirements for the
Degree of Bachelor of Science
in Aerospace Engineering
By

Cody Slater

and in Mechanical Engineering
By

Mariella Creaghan

Orland Lamce

January 7, 2016

Approved by:

Professor Nikolaos A. Gatsonis, Advisor
Aerospace Engineering Program, WPI

Jesse Mills, Affiliate Advisor
Group 75, MIT Lincoln Laboratory

Public Release: distribution unlimited. 16-MDA-8588 (2 March 16)
This material is based upon work supported by the Missile Defense Agency under Air Force Contract No. FA8721-05-C-0002 and/or FA8702-15-D-0001. Any opinions, findings, conclusions or recommendations expressed in this material are those of the author(s) and do not necessarily reflect the views of the Missile Defense Agency.

Abstract

This project presents the design and fabrication of a hydrogen peroxide six-axis propulsion system for picosatellites. An experimental test setup is designed and fabricated with a torsional thrust stand for measurements of the steady-state thrust. The setup includes a thrust block, a catalyst block, a feed system, and sensors for measuring the chamber pressure and temperature. Safety procedures are established. The optimum catalyst bed-length is established with analytical modeling assuming operation with 98 weight percent hydrogen peroxide. Nitrogen, helium, and water pressurization tests are performed as well as a nitrogen firing test and a valve-actuation test. Experimentation under atmospheric conditions and a chamber pressure of 95 psia shows approximately 0.6 N of thrust.

Acknowledgements

The team would like to give a special thanks to all those who helped make this project possible. These people believed in our success from the beginning and worked hard to assist in our accomplishments. Tremendous gratitude goes towards:

- Jesse Mills for his advice and oversight.
- Adam Shabshelowitz his continual contribution of great ideas.
- Kurt Krueger for always being ready to help with ideas or fabrication.
- Sean Crowley for his interest, contributions, and answering all our questions.
- Bakari Hassan for all his help on the catalyst bed model.
- Mark Seaver for his help with a driver circuit.
- Sharon Hardiman for helping us procure all our parts and always bringing snacks.
- John Howell for his help leak testing and wiring.
- Ted Bloomstein for believing in us.
- Ted Mendum for the use of his laboratory.
- Professor Gatsonis for advising from the WPI side.
- Professors Clancy and Brown for organizing the program.
- Jocelyn O'Brien for listening, encouraging, and always bringing a smile to our office.

Authorship Page

Project Subcategories:

CanSat System Design*
Task Led By: Cody Slater and Orland Lamce

Nozzle Design
Task Led By: Orland Lamce

Catalyst Bed Design
Task Led By: Cody Slater

Ground Support Equipment Design and Fabrication
Task Led By: Mariella Creaghan and Cody Slater
Assisted By: Orland Lamce

Component Procurement
Task Led By: Orland Lamce and Mariella Creaghan

Data Acquisition and Electronics Setup
Task Led By: Mariella Creaghan
Assisted By: Orland Lamce and Cody Slater

Experiment Design
Task Led By: Cody Slater
Assisted By: Mariella Creaghan and Orland Lamce

Experiment Setup
Task Led By: Cody Slater and Orland Lamce
Assisted By: Mariella Creaghan

Paper Authorship
Mariella: Introduction, Background, Ground Support Equipment, and Test Results and Discussion
Orlando: Background, CanSat Objective Configuration, Design of the Thruster Block, and Appendices A - G
Cody: Objectives and Methodology, CanSat Objective Configuration, Design of the Thruster Block, Test Results and Discussion, and Conclusion

Table of Contents

List of Tables

1 Introduction

Satellites have become an integral part of the modern American lifestyle. From the GPS navigation found in cars to television broadcast around the world, satellites have revolutionized communication, weather forecasting, and navigation for people across the globe. As satellite utility has skyrocketed, the number of satellites in orbit has increased to the over 1200 satellites currently in orbit today. In past years, launching a satellite into orbit was a large, expensive undertaking, requiring many millions of dollars and specially designed launch vehicles. However, since the introduction of the CubeSat, many research organizations and universities have been able to launch small satellites into orbit with low budgets via NASA's CubeSat Launch Initiative (CSLI). As technology has gotten more compact, many of the larger satellite components can now be replaced with much smaller ones, making small satellites, such as CubeSats, a more attractive option.

Although much of the technology used in satellites has been miniaturized since its introduction, one aspect of small satellites that has lagged is a highly maneuverable, compact propulsion system. Currently, small satellite propulsion has been focused on attitude control, not orbital control. Magnetic control has been the most widely used option, with roughly 60% of small satellites using these devices for attitude control. However, only 9% of operational small satellites are equipped with an orbital control system [Bouwmeester, 2010], the most popular being a cold gas propulsion system. Only one small satellite currently in orbit as of 2010 has a chemical propulsion system [Bouwmeester, 2010].

MIT Lincoln Laboratory's small satellite program has identified the need for a propulsion system capable of fitting inside a small satellite weighing approximately 1 kg. Since Lincoln Laboratory has a previously developed ejector system, similar to the common ejector used for

CubeSats, the volume restrictions of this system create a need for a propellant with a high volumetric impulse. Due to the volume constraints of the system, a cold gas propellant would not be sufficient for such an application. Similarly, bipropellant systems are traditionally less compact because of the need to store an oxidizer as well. The choice left is that of a monopropellant system, and after comparing different monopropellants, hydrogen peroxide was the propellant of choice because it has a high volumetric impulse, is relatively safe to test in-house, and is readily available for immediate development.

The goal of this Major Qualifying Project (MQP) conducted at MIT Lincoln Laboratory (MIT LL) is to design and build a fully functional and testable hydrogen peroxide thruster that could be integrated into a picosatellite. MIT LL provided the basic requirements for a propulsion system that could be applied to a variety of small satellite applications. From these, an appropriate catalyst bed and nozzle was designed, theoretically meeting or exceeding these requirements.

To test and prove the concept of the hydrogen peroxide propulsion system, a fully integrated test platform was designed and built with thrust, temperature, and pressure measurement capabilities. The design and manufacture of a thrust stand and thrust block to contain the catalyst bed and nozzle was also pursued. This project included the determination of the optimum length of the catalyst bed for fully decomposing hydrogen peroxide through empirical experiments using the geometry specified. The system tests were initialized with nitrogen gas firing to test for leaks and verify all the sensors worked properly. The system test was then performed with water to verify. The final tests determined the performance of our hydrogen peroxide thruster and provide a direction for future work.

Overview of Small Satellites

Satellites and spaceflight began during the space race between the United States and the former USSR. The ambition of each nation to become the first to reach flight at extreme altitudes gave way to the concept and design of various spacecraft [Schefter, 1999]. Satellites were, per Eisenhower's announcement, the United States' contribution to the International Geophysical Year (IGY)—a program that marked the Cold War's end by once again resuming the scientific interchange between the East and West [IGY, 2001]. The IGY tasked 67 nations to cooperate scientifically and advance understanding of "our earth, our atmosphere and…the future of the Antarctic Continent [IGY, 2001]." Yet all the IGY truly accomplished was to draw the starting line for the race into space—and the Space Age.

The first artificial satellite to orbit Earth, Sputnik 1, shown in Figure 1, marked the beginning of the Space Age on October 4, 1957 [Siddiqi, 2003]. What first started as a race gradually became an endeavor to learn more about the Earth and the Universe. Some of the sciences that helped inspire the role of satellites were meteorology, space physics, heliospheric physics, astronomy, precision mapping of the Earth, and oceanography to name a few. This unprecedented, continuous capture of scientific data propelled man's understanding of the universe forward.

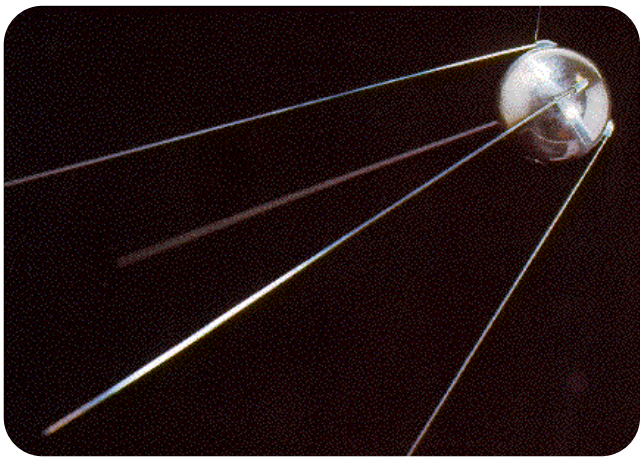

Figure 1. The first artificial satellite was *Sputnik*, launched by the former USSR [Courtney, 1998].

Yearly satellite launches, which had been declining since the mid-1990s, again begin to climb after the turn of the century as depicted by the visual representation of NASA records in Figure 2. One major difference though was their size. To establish a baseline, the mass of the International Space Station is over 419,000 kg. Smaller, single piece satellites include the Hubble Space Telescope at 11,110 kg and the Voyager spacecraft weighed in at 733 kg [Frost et al, 2014]. Advances in technology have made it possible to miniaturize almost every aspect of a satellite. From communication and navigation to processing and data collection, the size of a functional satellite is now orders of magnitude smaller than in the recent past. This decreases the cost of developing and launching a satellite, allowing more satellites to be placed in orbit. Constellations of these small craft can even be used to regain the full functionality of a larger machine.

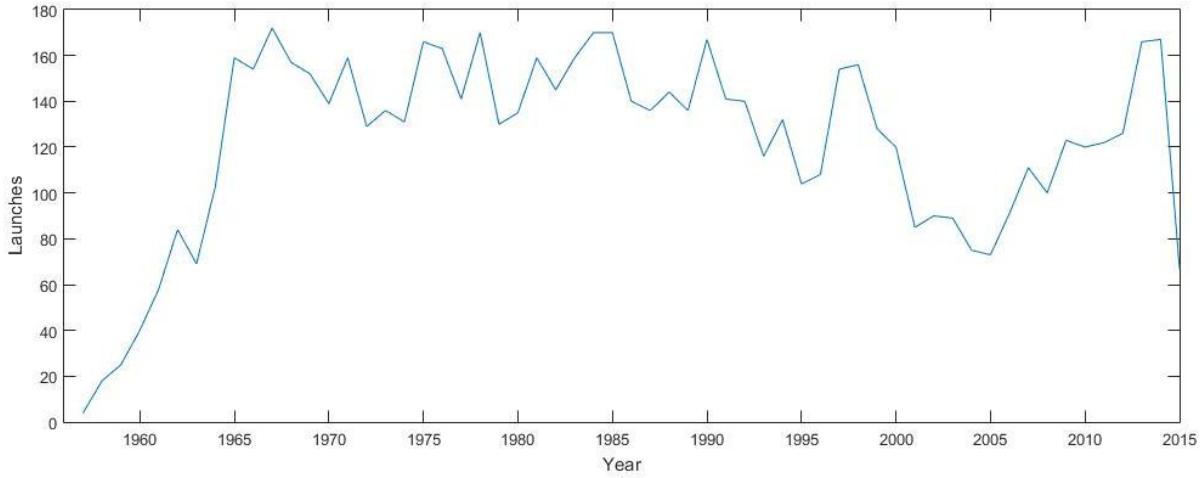

Figure 2. Launch data since the 1950s indicates a current trend upwards in satellite launches. Launch data provided by NASA.

The recent trend in small satellite developments has been quantified by NASA, breaking down the categories for "small" satellites. Figure 3 expands on modern satellite sizing, with the smallest category referred to as picosatellites. In general, small satellites are low in mass, under 500 kg, requiring lower thrust to maneuver in space. The CubeSat has become the flagship of small spacecraft because of the relatively low development costs and timelines involved in implementing a mission with these vehicles.

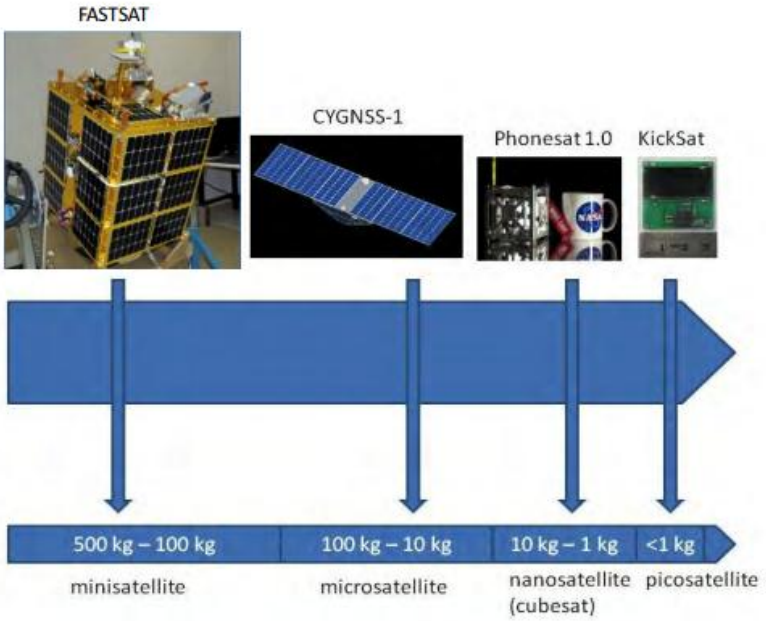

Figure 3. NASA has conducted work on classifying these small satellite categories [Frost et al, 2014].

Particular emphasis is often placed upon the mass, cost, and system capability during satellite development. There is a specific trade-off between spacecraft size and functionality, though miniaturization and integration technologies have answered this issue for a large part [Frost et al, 2014]. Cost remains an active factor in planning for the launch of a spacecraft however. The technological advancements in the past two decades have created space-grade commercial-off-the-shelf (COTS) components and consumer electronics that are cheaper, more

capable, and fit the volume constraints small satellites face. Given the explosion in technological development during the space age, these components often perform even better than their original, expensive predecessors [Frost et al, 2014]. Small satellites have played an increasingly important role in the flight of space experiments. In fact, micro-electromechanical systems (MEMS), with components of "…microscale features, provide higher accuracy [of the instrumentation] and lower power consumption", which in turn has increased mission successes in the past [Frost et al, 2014]. Such demands for smaller satellites to match the capabilities of their larger counterparts depend on current and developing technologies for enabling advanced tracking, telemetry, command, and monitoring in small spacecraft. The method of approaching these problems was to reduce satellite dimensions; allowing a larger number of satellites to be launched per payload vehicle [Frost et al, 2014].

1.1 The CubeSat Approach to Accessing Space

The CubeSat was jointly proposed by California Polytechnic State University and Stanford University in 1999, as a means of research and exploration of Low Earth Orbit (LEO) [Messier, 2015]. A 1U CubeSat is defined as a spacecraft with a volume of 1 liter and mass just over 1 kg [Mehrparvar, 2014]. The standardized terminology regarding CubeSats is based on single units (U). The 1U spacecraft is the most basic unit, composed of a 10 cm cube. Combinations of this basic unit make up various sizes; Figure 4 displays the three most common frames for CubeSats.

Figure 4. The standard frames for a CubeSat center on the compilation of single units (1U) [Mehrparvar, 2014]

By definition, CubeSats fall into the lower end of nanosatellites, the second smallest classification of satellites. The hardware and power system costs for a CubeSat are much cheaper, lending themselves to use in academia, where funding falls significantly short of that needed to develop a larger satellite [Frost et al, 2014]. Even though CubeSats began as an academic endeavor, many companies around the world, such as Aerospace Corp., Surrey Satellite Technologies Ltd. (SSTL), etc., have adopted the design and produced different applications for these small satellites. An endeavor from NASA's Small Spacecraft Technology Program is the PhoneSat, which is most noted for sending a COTS smartphone and Arduino platform into LEO. This nanosatellite utilized the CubeSat 1U chassis and only cost $3,500 for the first version. Its primary mission was "staying alive in space, sending back digital imagery of Earth and space via its camera, while also sending back information about the satellite's health" [Klint, 2013]. The popularity of CubeSats has even spread into popular culture, with Popular Science featuring an article on the PhoneSat project in 2012 [Klint, 2013].

There are a number of CubeSat missions that would benefit from the installation of a highly capable propulsion system. One such mission involves flying an array of CubeSats to

form a communication system, removing space trash or older satellites by degrading their orbits, repairing or refueling expensive satellites, or even interplanetary exploration at a lower thrust.

1.2 Overview of Small Satellite Propulsion

Currently the majority of CubeSats are funded for educational research purposes. These feature little, if any means of maneuvering once in orbit. As government and industry use of nanosatellites, particularly the CubeSat concept, increases, propulsion requirements have sparked the research and development of miniaturized propulsion systems, effective for smaller satellites. A team at NASA's Jet Propulsion Laboratory undertook a review of all emerging micropropulsion technologies which are listed in Table 1 [Mueller et al, 2010]. However, review was limited to the technologies that the NASA team deemed most promising.

Table 1. NASA has conducted work on reviewing a complete list of emerging micropropulsin technologies [Mueller et al, 2010]. The most promising are outlined in this table.

Chemical Propulsion Thrusters	Electric Propulsion Thrusters	Propellant-less Propulsion
Hydrazine Thrusters	Pulsed Plasma Thrusters (PPTs)	Electromagnetic Formation Flying
Hydrogen Peroxide Thrusters	Vacuum Art Thrusters (VATs)	Electrodynamic Tethers
Cold Gas Thrusters	Miniature Hall Thrusters	Solar Sails
Butane Thrusters	Miniature Ion Engines	
Solid Rocket Motors	Electrospray Thrusters – Colloid, FEEP	
Digital Microthruster Arrays	Resistojets	
Bipropellant Thrusters	Microcavity Discharge Thrusters	

Monopropellant Thrusters

Within the category of chemical micropropulsion systems, monopropellant thrusters, a mainstay for current macro-scale propulsion, are the focus of many miniaturization efforts. Current monopropellant systems rely primarily on hydrazine and hydrogen peroxide as fuel, with hydrazine being the most prevalent. However, due to recent interest in hydrogen peroxide as a non-toxic propellant, the use of hydrogen peroxide has resurged, as it was a popular propellant choice in the 1960s space era [Mueller et al, 2010].

The thrust generated by a monopropellant system is based on the exothermic catalytic decomposition of the propellant into hot gas which then flows through a converging-diverging nozzle, expanding the gas and generating thrust. Hydrazine decomposes into ammonia, nitrogen and hydrogen, while hydrogen peroxide decomposes into oxygen and superheated steam. The diagram in Figure 5 illustrates this basic concept.

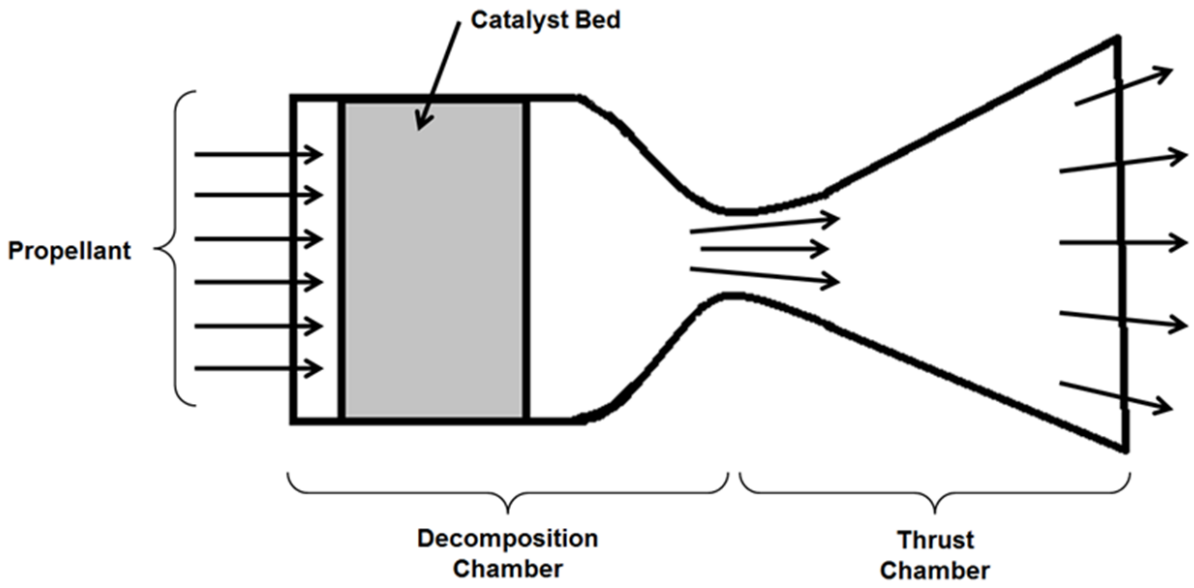

Figure 5. Monopropellant thrusters work through the expansion of gases created by the exothermic decomposition of propellant.

A monopropellant system that could, with minimal modifications, be used with both hydrazine and hydrogen peroxide was designed and tested by Donald Platt [2002]. The design also included a unique twisted mesh catalyst bed constructed of iridium/alumina for the hydrazine thruster and silver for the hydrogen peroxide thruster. The hydrazine system had a minimum impulse bit of 1.715×10^{-4} N-s and specific impulse of 150 sec [Platt, 2002]. The hydrogen peroxide thruster testing was not completed but early results showed that it was achieving full decomposition and the performance should be less than, but close to that of hydrazine [Platt, 2002].

Cold Gas Thruster

Cold gas thrusters are the simplest of these propulsion choices. They have been space proven since the 1960s and offer good reliability, albeit lower performance than a monopropellant thruster, with specific impulses at around 65 sec, compared to 150 sec [Mueller et al, 2010]. However, a drawback of these systems is that they are often large, heavy, and bulky, since the highly pressurized gas requires a sturdy tank [Mueller et al, 2010].

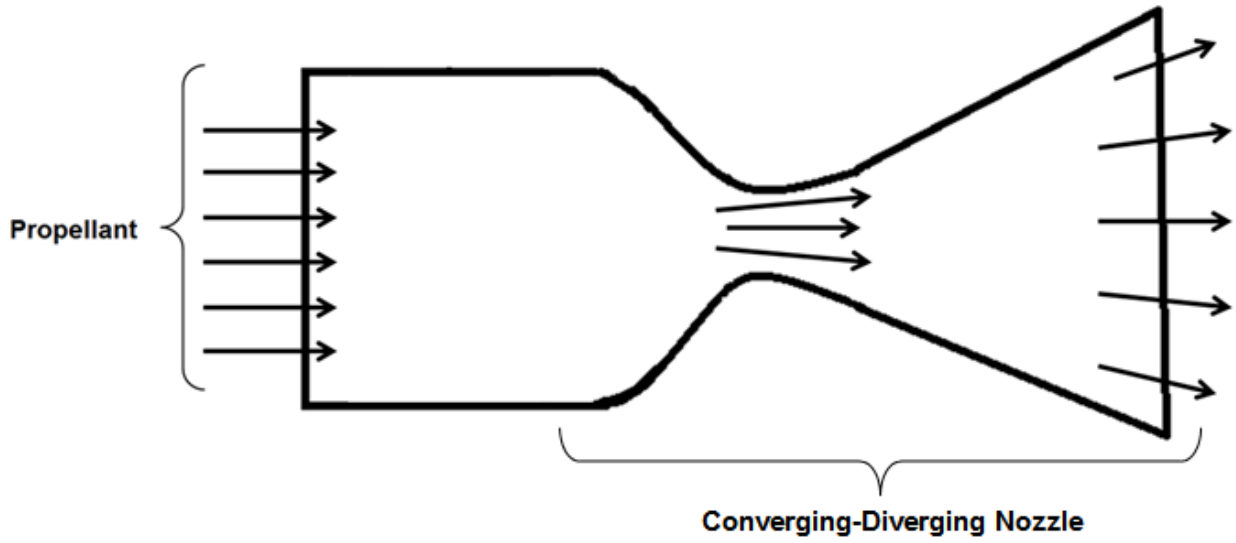

Figure 6. A cold gas thruster operates through expanding a gas from an area of high pressure to an area of low pressure via a converging diverging nozzle.

A cold gas thruster, shown in Figure 6, works by releasing a highly pressurized cold gas, typically nitrogen, through a valve to a converging-diverging nozzle, generating thrust.

An advantage to cold gas thrusters is that there are many COTS nozzles available for use, lowering development costs. However, the size, weight and power requirements of these systems limit their use in nanosats and picosats.

Butane Thrusters

Butane thrusters operate under a similar premise as a cold gas thruster, except that the butane is stored as a liquid in the tank and transfers into the gas phase upon expansion. Butane thrusters were introduced into the space industry in 2000 when they were flown on the SNAP - 1A mission from England [Mueller et al, 2010]. However, NASA's Jet Propulsion Laboratory later created a butane thruster design for CubeSat applications. The low vapor pressure of butane and the low (under 100 psi) pressure needed in the entire system is an advantage to a butane

system. However, the specific impulse of the butane CubeSat propulsion system was only around 70 sec, and the thrusters produced a maximum of 25 mN of thrust [Mueller et al, 2010].

VACCO developed a self-contained Micro-Propulsion System (MiPS), specifically designed for use in CubeSats, featuring five thrusters, tanks, valves and sensors all fully integrated into a system. Overall, butane thrusters provide good low delta-v service for attitude control on CubeSats [Mueller et al, 2010].

Pulsed Plasma Thrusters

In the electric propulsion realm, pulsed plasma thrusters (PPTs) are becoming popular for research in micro electric propulsion systems. As explained by Mueller:

"In a PPT, a capacitor, connected to two thruster electrodes, is charged and a discharge is triggered between these two electrodes. The ensuing arc ablates Teflon material off the solid fuel rod. This ablated material, due to Lorentz forces as a result of the current flowing through the plasma generated between the electrodes and its interaction with its surrounding self-generated magnetic field, accelerates and is expelled from the thruster".

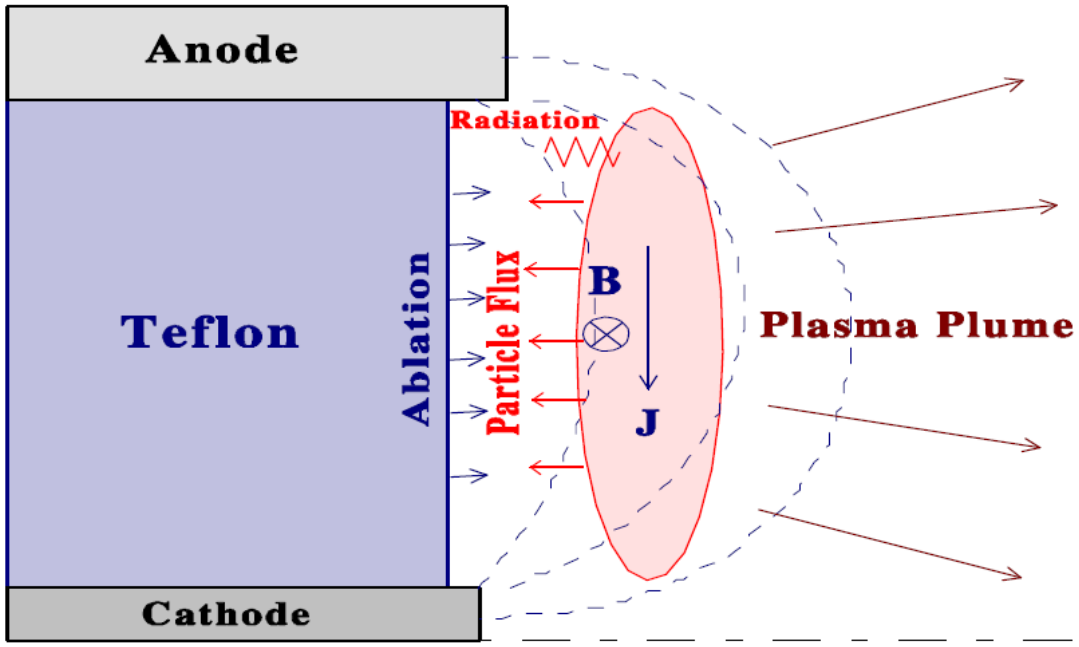

Figure 7. A pulsed plasma thruster ablates particles of Teflon between two electrodes [Spanjers, 2002].

The Air Force Research Laboratories developed and tested a MicroPPT for 25 kg microsatellites which generated 2-30 μN of thrust while the system had a mass of 500 g [Spanjers, 2002]. Although this system is currently not fit for use on CubeSats, development in PPTs is increasing, especially in the realm of using PPTs for attitude control on CubeSats. In fact, a study was conducted by Gatsonis et al [2015] showed that μPPTs can be used for for attitude control on a CubeSat and that it would achieve high pointing and attitude accuracy [Gatsonis et al, 2015].

Vacuum Arc Thrusters (VATs)

Vacuum Arc Thrusters are another electric propulsion concept for CubeSats. VATs shown in Figure 8 generate thrust by creating an electric arc between a cathode and an anode,

which causes cathode material to be ejected at high velocity creating a low-thrust propulsion system [Rysanek et al, 2002]. The University of Illinois developed a 3U CubeSat which included a μVAT system for attitude control; however the satellite was destroyed upon launch vehicle failure in 2006.

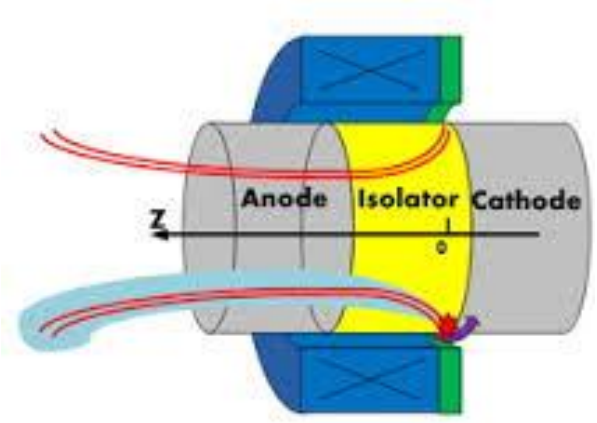

Figure 8. A vacuum arc thruster operates by ejecting cathode material.

The advantages of a VAT for a small satellite include the propellant being stored in the thruster head, making compact configuration possible. However, the VAT can produce only small amounts of thrust, making the VAT more suitable for precision pointing and attitude control, but not axial bussing.

Miniature Ion Engines

Miniature ion engines, typically using xenon gas as a propellant, generate thrust by extracting ions from plasma which is generated in a discharge chamber [Mueller, 2010]. Although not specifically designed form CubeSat missions, Micro-Ion engines have produced 0.001-1.5 mN of thrust while only being 2-3 cm in diameter. Pennsylvania State University has developed and tested a Micro Radio-Frequency Ion Thruster system using argon gas for initial testing, however they plan to ultimately use xenon.

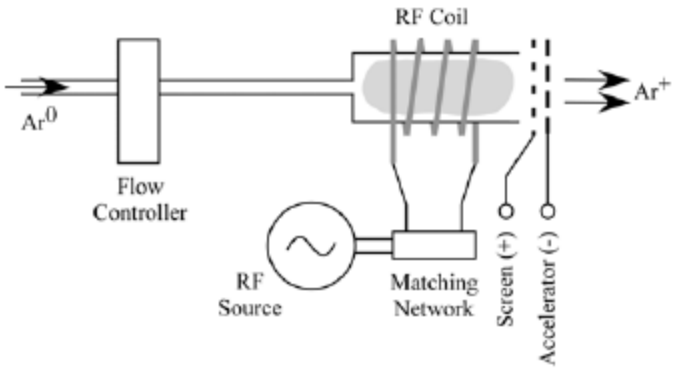

Figure 9. The thruster developed by Penn State uses micro-ion technology to generate low thrust.

The maximum thrust that the Penn State thruster achieved was 59 μN and a specific impulse of 5480 s [Trudel et al, 2009]. Micro-ion propulsion systems for CubeSats specifically have yet to be developed, however future concepts include possibly developing a contained system that could fit in 1U of a 3U CubeSat [Mueller et al, 2010].

Electrospray Thrusters

Electrospray thrusters consist of a propellant feeding up into an emitter, where an opposing electrode creates an electric field between it and the emitter. The electric field strengthens and depending on the type of electrospray thruster, ions or charged liquid droplets are extracted from the propellant [Mueller et al, 2010]. Ion-extracting thrusters are known as Field Emissions Electric Propulsion (FEEP) thrusters, while droplet-extracting thrusters are known as colloid thrusters.

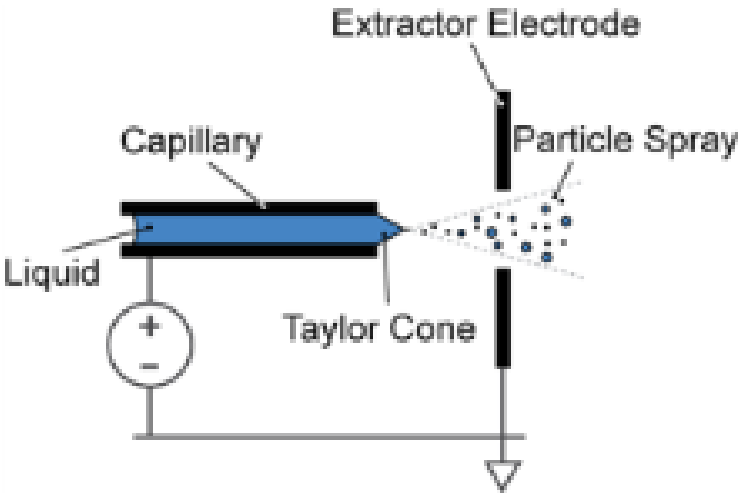

Figure 10. Electrospray thrusters operate by discharging ions in an electric field [Mueller et al, 2010].

Electrospray thrusters offer thrust on the scale of μN to mN, and current designs are quite large for a CubeSat application. However, with further development, electrospray thrusters could allow substantial maneuverability of a CubeSat [Mueller et al, 2010].

Monopropellant Thrusters: Why Hydrogen Peroxide?

For the picosatellite applications of interest to this MQP, we limited our search to monopropellants because of the size constraints. Monopropellants only require the propellant and a catalyst bed in order to operate, reducing the total volume of the propulsion system. Although cold-gas thrusters have a low volumetric impulse, nitrogen gas was also investigated in order to compare a previously developed propulsion system used in MIT-Lincoln Laboratory's satellite program. A comparison of the monopropellants considered is shown in a stoplight chart in Table 2 below:

Table 2. A comparison of the most promising propellant options were organized into a stop light chart for a side-by-side comparison.

	Volumetric Impulse (kg*s/m^3)	Ground Infrastructure	Test Precautions	Attainability	Flight Proven
Nitrogen Gas	33,314	Cheap, abundant materials	Minimal precautions needed	Easy to obtain	Used on previous application
Hydrazine	234,600	Expensive, complex, limited materials	Carcinogenic, difficult to handle	Relatively easy to obtain	Standard propellant choice
"Green" Monopropellants	~400,000	Yet to be developed	Reactive, handling requires special precautions	Newly developed	Still in development
Hydrogen Peroxide	215,298	Relatively cheap, limited materials	Highly reactive, handling requires special precautions	Easy to obtain	Popular in 1950s and 1960s

Hydrazine [N_2H_4] is a toxic monopropellant used in the majority of monopropellant thrusters. It is a strong reducing agent and has high performance. However, due to its high toxicity, testing of a hydrazine thruster would require extensive safety precautions and an experienced handling infrastructure. Figure 11 shows the GHS classification for hydrazine, exemplifying the hazards. Hydrazine decomposes into a toxic mixture of nitrous oxide and ammonia, requiring containment after decomposition. These hazards make hydrazine undesirable for our use as a propellant because we need to be able to test it in-house while minimizing development costs.

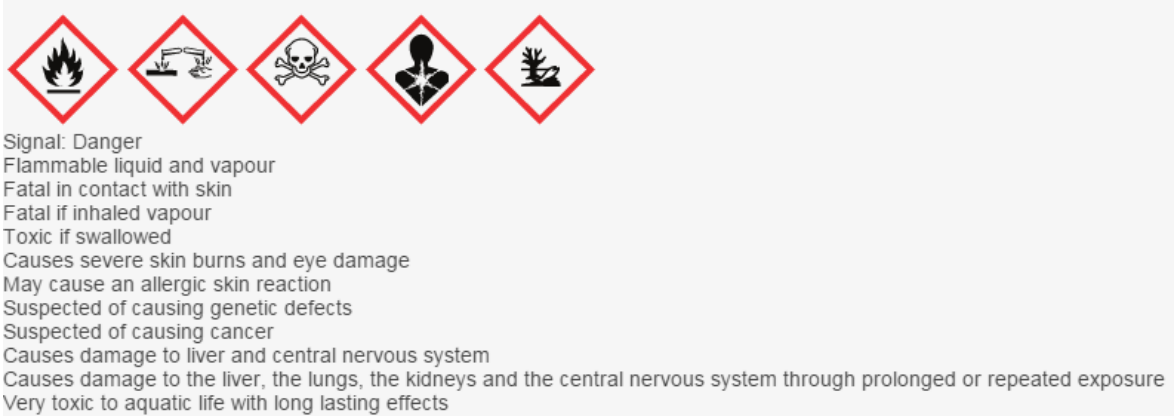

Figure 11. The GHS classification of hydrazine illustrates the dangers of its use [LabChem Inc, 2013]

Green Monopropellants, such as AF-M315E, developed at Air Force Research Laboratories at Edwards AFB, CA, are the newest type of monopropellants and are still in the process of being established and tested. The development of these monopropellants is focused on safety of handling, while having performance parameters similar to that of hydrazine. The AF-M315E monopropellant is still in testing, but it is predicted to have greater than 150% of the performance of hydrazine [Hawkins et al, 2010]. NASA is expected to complete in-orbit testing of the monopropellant later this year. Although the green monopropellants could possibly complement our application, the lack of research and flight testing has led us away from the green monopropellants. These may be appropriate for future solutions, however the large research costs up front would minimize the ability to provide MIT Lincoln Laboratory an immediate, inexpensive solution.

Hydrogen Peroxide has long been used as a propellant, since 1935 when Hellmuth Walter first concentrated it to 80% and experimented with it as a submarine turbine drive system [Wernimont et al, 1999]. The use of hydrogen peroxide as a rocket propellant became very popular in the United States in the 1940s – 1960s, primarily in monopropellant thruster applications. A notable example is the Mercury spacecraft, which contained sets of hydrogen

peroxide attitude control thrusters. Hydrogen peroxide, however, was phased out in the 1970s and 1980s in favor of the better performance of hydrazine. A renewed interest in environmentally-friendly and biologically safe propellants in the 1990s caused hydrogen peroxide to reemerge as a viable alternative to hydrazine. Not neglecting the shortcomings of hydrogen peroxide, it does have a lower volumetric impulse than hydrazine and must be handled with an increased level of caution. Figure 12 highlights the GHS classification of hydrogen peroxide. This propellant gains favor in that it does not come with the carcinogenicity, toxicity, or flammability of hydrazine. Hydrogen peroxide also decomposes to vapor and oxygen gas.

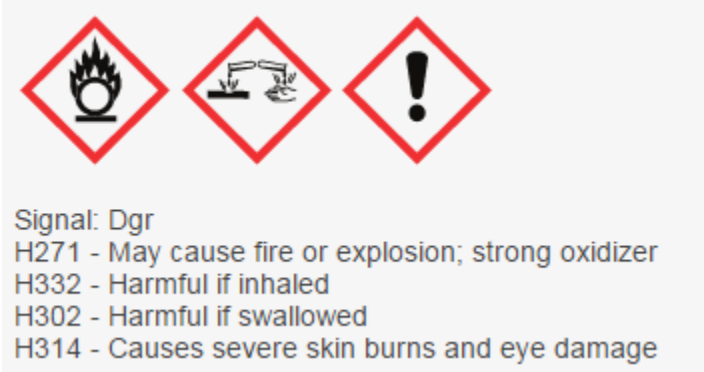

Figure 12. The GHS classifcation of hydrogen peroxide indicates relative caution needed [LabChem, 2012].

Since the resurgence of hydrogen peroxide as a safe propellant, a number of efforts have been undertaken to develop a new set of thrusters built for small spacecraft, scaling down the ones built in the 1940s-1960s. For use in a flight system, the weight percent of hydrogen peroxide will be chosen so as to maximize the propellant's performance. Accordingly, the actual application will depend on 98 weight percent peroxide and all of the calculations in this project assume this. However, due to the long lead time to obtain the 98 weight percent, the actual

peroxide used in the test firings in our project was 86 weight percent. To develop proper procedures we reviewed three thruster designs and analyzed their test efforts as case studies.

Case Study I: Development of a 100-Millinewton Hydrogen Peroxide Microthruster

A 100-Millinewton hydrogen peroxide monopropellant microthruster was developed by Kuan et al [2007]. The objectives were to develop and test a 100 mN thruster to serve as the attitude control system for micro spacecraft and to study the issues associated with miniaturization of hydrogen peroxide thrusters. The thruster parameters were chosen using traditional analytical methods assuming steady-state isentropic flow through the nozzle, ideal gases, and neglecting friction and boundary conditions. The nozzle was designed for the thrust of 100mN and ambient pressure of 101.3 kPa. The resulting properties of the nozzle are summarized in Table 3 below:

Table 3. Nozzle parameters for the 100mN hydrogen peroxide thruster.

Thrust	100 mN
Mass Flow Rate	0.18 g/s
Throat Diameter	0.5 mm
Exit Diameter	0.7 mm
Expansion Angle	15 deg
Chamber Pressure	109 psi

Silver was selected as the best catalyst material for this study using 92% hydrogen peroxide. Three different catalyst configurations were initially tested: silver coated aluminum oxide pellets, 1 mm diameter silver pellets and pure silver flakes (90-250 μm). 0.7 g of silver flakes buffered by two fine aluminum screens was chosen as the best catalyst. A thrust stand accurate to millinewtons was developed for testing purposes. The test stand consisted of a suspended flat plate containing the entire system. Thrust was measured via deflection of a thin copper strip measured by strain gauges. It was calibrated prior to every test and was found to be accurate to 1 mN. The nozzle and catalyst bed enclosure was made from 316 Stainless Steel with Viton seals. Kuan et al [2007] investigated the thruster's ignition delay time by activating the solenoid control valve once the catalyst bed reached a prescribed temperature. Pressure and temperature were measured downstream of the catalyst bed and the decomposition efficiency was estimated from these values. Kuan et al [2007] measured the thrust at a preheating temperature of 420 K where the ignition delay was less than 50 ms by opening the valve at 500 ms and closing it after 10 s. The tests found that the ignition delay was the shortest (0.035 s) when preheated to 453 K and that 90% c* efficiency can be achieved with 92% hydrogen peroxide at a flow rate of 0.18 g/s. The thruster generated 182 mN and had a specific impulse bit of 101 s when tested under atmospheric conditions.

The Design, Development and Test of One Newton Hydrogen Peroxide Monopropellant Thruster

The objective of Amri et al [2012] was to develop and test a one newton monopropellant thruster using a green monopropellant, as well as to test different catalyst configurations. The nozzle design was hinged on a thrust requirement of 1 N, and 11 bar (156 psi) chamber pressure,

and the 722.6 C decomposition temperature of 89% hydrogen peroxide. The resulting nozzle parameters are summarized in Table 4, below.

Table 4. Design parameters of a 1 N hydrogen peroxide thruster.

Thrust	1 N
Mass Flow Rate	0.68 g/s
Throat Diameter	0.8 mm
Exit Diameter	8.0 mm
Expansion Angle	15 deg
Chamber Pressure	156 psi

The catalyst chosen was a pack of ½" diameter silver mesh screen disks of varying lengths and disk counts. The team tested catalyst bed lengths of 10 and 20 mm each with 50, 60 and 100 mesh disks and found that the 10 mm length with 60 disks provided the best decomposition indicated by decomposition temperature. The temperature and pressure were measured after the catalyst bed but before the nozzle. The tank pressure and temperature were also recorded as well as the feed pressure and catalyst temperature. The specific impulse and thrust were calculated from these measurements.

After pressurizing and filling the tank, the catalyst was preheated by pulsing hydrogen peroxide into the catalyst bed until the specified temperature was reached. The peroxide was then flowed through the system at the specified mass flow rate until thermal equilibrium was reached,

when the test stopped. This was repeated for different preheating temperatures and catalyst bed configurations.

The thruster provided the best performance with the most densely packed catalyst bed that still had an acceptable pressure drop. This was 100 silver mesh disks in a 10 mm catalyst bed. This configuration had a specific impulse of 170 s (greater than objective 150 s) and a mass flow rate of 0.8 g/s. However, the thrust was about 1.4 N instead of the 1.55 N expected for a test at 17 bar. Overall the thruster gave good performance and demonstrated its ability to replace toxic monopropellant thrusters.

MEMS-Based Satellite Micropropulsion Via Catalyzed Hydrogen Peroxide Decomposition

Hitt and Zhou [2002] of this work was to develop a MEMS-based, catalytic monopropellant thruster which uses HTP as the liquid propellant. The thruster nozzle was designed using the usual analytical methods for a thrust level of 500 μN. The following table shows the parameters for the nozzle.

Table 5. Nozzle design parameters for a MEMS hydrogen peroxide thruster.

Thrust	500 μN
Mass Flow Rate	275 μg/s
Throat Diameter	30-90 μm
Expansion Angle	15-20 deg
Chamber Pressure	5-6 psia

Silver was chosen as the catalyst material. The length of the catalyst bed was determined from scaling macroscale HTP thruster catalyst beds to MEMS scale, resulting in an estimate of

1.7-2 mm. The design of the catalyst bed was a sequence of straight microchannels with 90 degree bends. A second design of diamond pillars was also manufactured. The channels were 29 μm wide and 50-300 μm deep.

The testing began with sending dyed water through a 1 mm diameter stainless steel tube epoxied onto the silicon chip in which the thruster was etched. Tests were all viewed and recorded under a microscope. The next tests involved ~80% hydrogen peroxide and the concentration was increased up to a targeted value of 90% hydrogen peroxide. The tests were performed with various catalyst chamber lengths and decomposition was measured via a refractometer.

The catalyst bed length which would have full decomposition is estimated to be 4 mm, not 2 as originally expected. The catalyst bed pillar design caused gas pockets to form and would choke portions of the flow inside the catalyst bed. These tests demonstrated the difficulty of making micronewton hydrogen peroxide thrusters. The primary difficulty was achieving complete decomposition within the MEMS geometry.

1.3 CanSat Objective Configuration

Expansion into small satellites, and particularly picosatellites, is a topic that is garnering interest at MIT LL. The concept proposed to our team was to create a satellite that could fit into a common ejector already used by the lab. This would require a cylindrical profile 4.5" in diameter and 5" in length. This led way to the development of the CanSat: a satellite bordering the edge between a picosatellite and nanosatellite at an estimated mass of 1 to 1.5 kg. The CanSat primarily exists as an exercise in developing our propulsion system. The purpose of the CanSat would be to demonstrate the functionality of a miniature monopropellant subsystem, while maintaining the ability to capture data and relay it to the ground while in LEO. Beginning with the specified geometry and resulting volume, the subsystems needed to control flight, gather data, and communicate with the ground were chosen from COTS parts, most with spaceflight

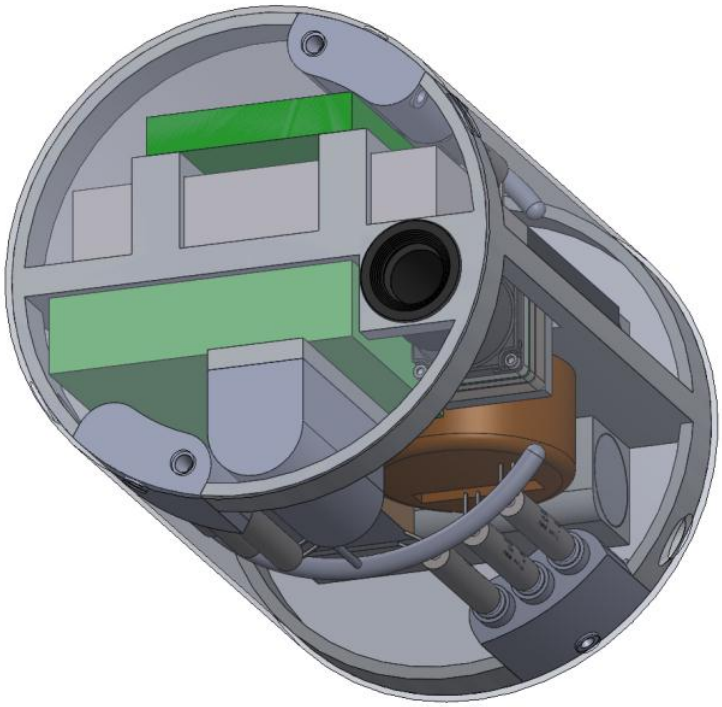

Figure 13. The concept of the CanSat was developed to provide volume constraints for a proposed picosatellite system. Propulsion system

heritage. The remaining space in the craft was reserved for the propulsion system and provided rough working requirements for the volume our propulsion system would need to occupy.

1.3.1 CanSat Components

The components for the CanSat were chosen to meet the basic requirements of controlling flight via an onboard computer, gathering data with an infrared sensor, receiving and transmitting data to the ground with a compact transceiver, and establishing a relatively precise location with onboard navigational devices. To satisfy these requirements, research was conducted in order to find suitable COTS components. The typical requirements of a picosatellite were considered and include low mass, power, and size. The minimum duration of for this proof of concept mission for the CanSat was set at 20 minutes. This would provide ample time to completely test the system performance. This mission duration was used to calculate the energy expenditure of the craft. Keeping these variables and the tight volume constraints in mind, the following components were chosen. Red numbers under energy represent power usage, while green indicate a power source.

Table 6. The notional design of a CanSat craft centered on the implementation of COTS components. A summary of the selected components and their energy requirements are presented in this table.

Unit	Make & Model	Mass (g)	Energy Expenditure (Wh)
Camera & Lens	FLIR Quark 2 w/ 19mm lens	23.8	**0.33**
Radio	L3 Micro-CDL	125	**1.33**
Amplifier	L3 RFE amplifier	100*	**3.96***
Computer	Xiphos Q7	24	**0.33**
Batteries	2 x Panasonic NCR-18650A	95	**22**

IMU	Sensonor STIM300	55	**0.66**
GPS	Rockwell Collins NavFire	80	**0.924**
Structure	Custom	400*	
Valve	The Lee Company IEP Series	56.4	**1**
Cables/Margin	Custom	400*	
TOTAL		1484.2	**12.136**

The Xiphos Q7 is an on-board computer used for high rate data compression and comes from a line of space qualified boards. The STIM300 is a small, non-GPS aided IMU, typically used in unmanned aerial vehicle (UAV) applications and has an assortment of MEMS sensors—3 axis gyros, 3 axis accelerometers, and 3 inclinometers. Because the selected IMU does not have built-in GPS capabilities, a separate GPS unit was selected—the Rockwell Collins NavFire. For capturing sample imagery, in the infrared spectrum, the FLIR Quark 2 with a 19 millimeter diameter lens was also settled on for gathering sample imagery to relay to the ground. A customized Micro-CDL radio and RFE amplifier were discussed with L3 West Communications and were chosen for the communication needs of the craft. To provide power to each component, two Panasonic NCR-18650A were selected. These are COTS industrial lithium ion batteries capable of providing the energy and voltage required for the sample mission duration.

1.4 Objectives and Methodology

The goal of this MQP is to design and build a fully functional and testable hydrogen peroxide thruster that could be integrated into a picosatellite. To accomplish this goal the following objectives and approaches established were:

1. Ensure the safety of all team members throughout each stage of testing.
    - Undergo basic laboratory and chemical safety training.
    - Undergo hydrogen peroxide safety training.
    - Follow precautions outlined in *Appendix C: Safety*.
    - Proof test milestones, as shown in *Appendix D: Laboratory Protocols*, must be satisfied before continuing subsequent testing stages.
2. Design, fabricate, assemble, and calibrate the following ground support equipment
    - Torsional thrust stand
    - Thrust block
    - Catalyst block
    - Catalyst bed and components
    - Valve rest plate
    - Blast shield
    - Acquire and assemble the necessary commercial off the shelf (COTS) components, valves, and pumps to create a closed test system.
    - Precision clean all components that will come in contact with hydrogen peroxide per MIT LL standards.
    - Passivate system critical components.

3. Proof test the system validity as a whole.
    - Following the procedures outlined in *Appendix D: Laboratory Protocols*, undergo a series of nitrogen proof tests which include:
        - Relief valve crack test with nitrogen.
        - System leak test with nitrogen.
        - Actuated relief valve performance test with nitrogen.
        - Nitrogen-firing sensor check.
4. Verify live-firing test procedures and safety.
    - To ascertain absolute safety of the loading procedure, load simulated H_2O_2 (H_2O) into the system via the procedure presented in *Appendix E: Loading the System*.
    - Implement revisions to eliminate liquid exposure to unintended surfaces.
    - Implement the simulant H_2O_2 pressurization process and conduct a variety of tests including:
        - System leak test with H_2O.
        - Actuated relief valve performance test with H_2O.
5. Perform empirical experiments to optimize the length of a catalyst bed with a specified geometry.
    - Flow 86 w% H_2O_2 through the catalyst block with varying catalyst lengths. Take exit temperature measurements for as many of the catalyst bed lengths below as time allows (.5 cm, 1 cm, 2 cm, 4 cm, 6 cm)

6. Live-fire the complete system and characterize the resulting steady state performance.
    - Fully integrate all components for a live-firing with H_2O_2. Test the system with the following configurations of volume of propellant: 50 mL at 100 psi starting feed pressure; 50 mL at 50 psi starting feed pressure; 50 mL at 30 psi starting feed pressure; 100 mL optimal starting feed pressure.

2 Design of the Thruster Block

This chapter presents the design process that resulted in the final configuration of a thrust block. A conceptual mission being planned by MIT LL drove the size, volume, and performance constraints of the system. The analysis and design of important components of the thruster were then undergone. These include the catalyst bed for decomposing propellant, a nozzle for expanding the flow, and a block capable of housing these components and functioning at the expected level.

2.1 CanSat Objective Design

In order to identify the functional space available in a generic picosatellite for use at MIT LL, a first order CanSat layout and system design was developed. This provided the foundation for developing a realistic model for the propulsion system. The notional assembly includes an objective thrust block, cylindrical fuel tank, dual manifold central feeds, and a triad valve arrangement. The size of the cylindrical fuel tank is flexible for specific mission requirements. One proposed method involves the integration of a spring with a high spring constant into the tank, which would act to pressurize the dual manifold central feed. This provides the six valves on the corresponding side of the craft with propellant. Each triad would house three nozzles, three catalyst beds, and connect to the three respective valves. An additional offset of 30 degrees of the top and bottom thruster block would be used to provide optimal control over the craft.

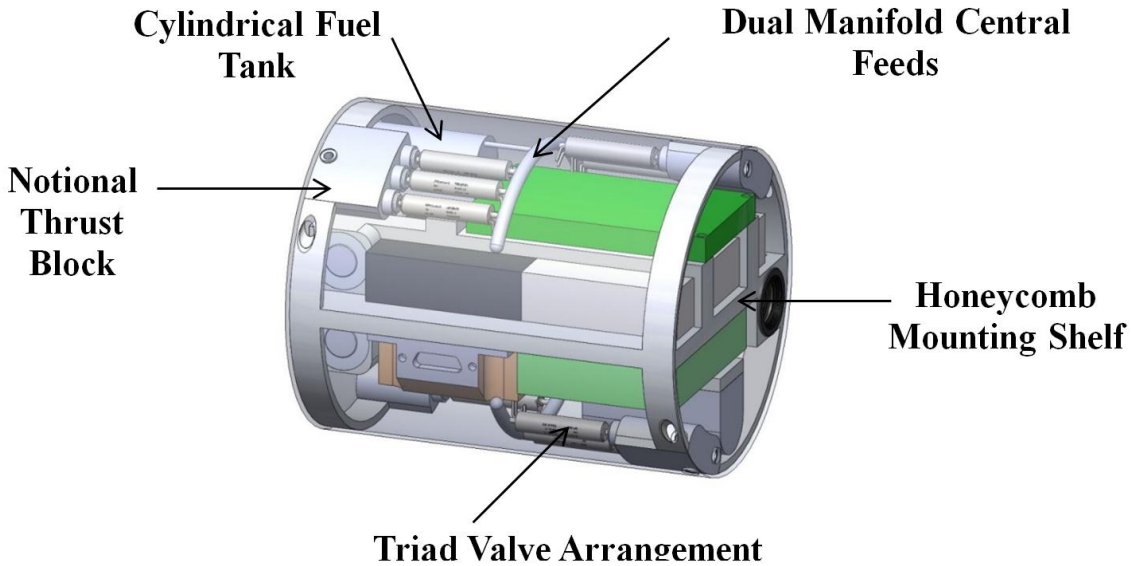

Figure 14. The objective propulsion system was designed to meet the volume constraints of the CanSat concept.

The experimental thruster block will be a derivative of the objective one. The primary purpose of the experimental thrust block is to reproduce an environment that would be realistically similar to that required on an actual spacecraft and in order to test the assembly itself. An increased margin of safety will also be present in the experimental thrust block.

2.2 Catalyst Bed Design

In monopropellant propulsion systems, the catalyst bed is responsible for the

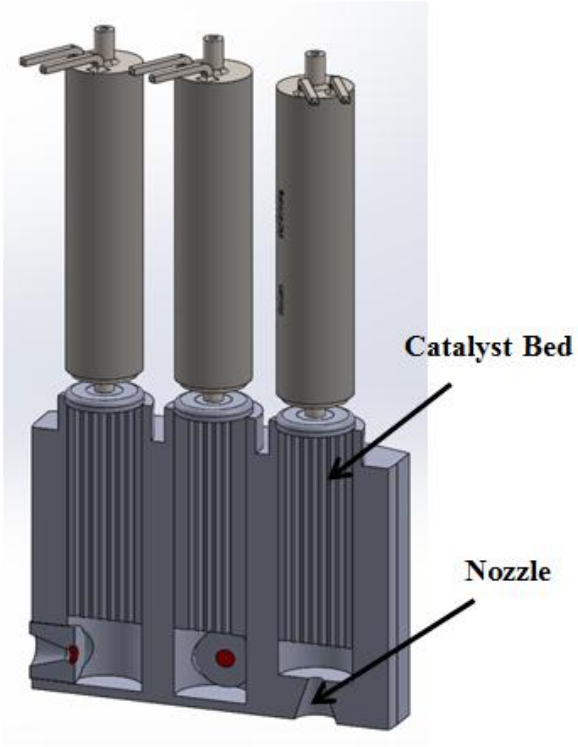

Figure 15. A design concept for the flight system centers on a triad design.

exothermic decomposition of the propellant. Catalyst beds come in a variety of proven configurations, each offering their own unique benefits. A few popular designs are included in Table 7.

Table 7. The five primary catalyst bed designs each serve to expose the propellant to the great surface area of catalyst.

Type of Catalyst Bed	Description
Pellet	Small pellets of catalytic material are packed between two retaining features.
Flake	Similar to a pellet design, flaked catalytic material is packed between two retaining features.
Mesh	Fine mesh grids are stacked to the appropriate thickness and typically compressed to increase mechanical properties.
Coated Composites/Ceramics	A composite, ceramic, or other appropriate material is coated with a layer of catalytic substrate.
Microchannel Cross Section	The catalyst bed cross sectional area is composed of numerous smaller microchannels through which propellant can flow.

For this specific application, decomposing hydrogen peroxide, a variety of materials exist for use as a catalyst. A complete list of materials that act as a catalyst on hydrogen peroxide can be found in *Hydrogen Peroxide* by Schumb, Satterfield, and Wentworth. However, the literature identified two standout materials for use in terms of reactivity, functionality, and versatility in rocket applications: pure silver and platinum [Schumb, 1955].

Both materials were considered for independent use, as well as for a substrate coating on a cordierite composite material, available commercially [Beutien, 2002]. In order to combat the degradation of performance that often occurs with catalyst beds, the solid metals were preferred, and the platinum option seems to hold the most potential in terms of performance. Silver was

chosen as the preliminary material given the significant time constraints and due to the relative ease of obtaining varying purities of silver.

Each catalyst bed presented in Table 7 was considered for use. The options were narrowed down immediately to the proven mesh catalyst beds, and the less explored microchannel option. Such designs were identified as the easiest to create from a manufacturing perspective. The initial design centered on machining several microchannel flow paths through a ¼" diameter pure silver rod of varying lengths. The channels would range from 750 to 1000 μm in diameter, depending on fabrication capabilities. Such a design offers several beneficial characteristics. Foremost, the single body structure provides unprecedented mechanical stability. Oxidation and wear on the catalyst bed over time will not negate performance as is the case when a coated substrate or fine mesh grid is used. Additionally, the microchannel approach would reduce the pressure drop experienced across its length. This is often an issue in pellet and flake catalyst beds, as the flow through is highly disrupted and turbulent.

2.2.1 Hydrogen Peroxide and Silver Interaction

The mechanism of reaction for silver decomposing hydrogen peroxide is still not well understood and has not been recently explored. The most complete analysis of the reaction kinematics and rates of reaction for silver and hydrogen peroxide was completed in 1963 by the Shell Development Company [Baumgartner, 1963]. This is an area that presents itself as an unexplored and interesting area of research in order for a more complete understanding to be reached.

The bulk decomposition of hydrogen peroxide when in the presence of silver occurs according to Eq. 3.1:

$$2H_2O_2(l) \xrightarrow{Catalyst} 2H_2O(g) + O_2(g) + \text{heat} \qquad (3.1)$$

The heat released during this reaction is dependent upon the molecular and atomic configuration of hydrogen peroxide. Referred to as the heat of reaction, this value is 54.14 kJ/mol. The specific amount of heat released gives rise to the adiabatic decomposition temperature of the fluid, which can be easily calculated for a given concentration of hydrogen peroxide. Appendix H contains MATLAB code that was developed to calculate heat of reaction and adiabatic decomposition temperature based on an input concentration. For 98 weight percent peroxide, the temperature of the products can be estimated at 1219 K.

As hypothesized by Baumgartner et al in 1963, a more complete description of the interaction of silver and hydrogen peroxide can be broken into the series of reactions outlined below.

$$Ag + H_2O_2 \rightarrow AgOH_{surf} + OH \quad (3.2)$$

$$OH + H_2O_2 \rightarrow H_2O + HO_2 \quad (3.3)$$

$$AgOH_{surf} + HO_2 \rightarrow Ag + H_2O + O_2 \quad (3.4)$$

$$AgOH_{surf} + H_2O_2 \rightarrow Ag + HO_2 + H_2O \quad (3.5)$$

$$AgOH_{surf} + 2(H_2O_2) \overset{\rightarrow}{\Leftrightarrow} Ag^{+}(H_2O_2)_2 + OH^{-} \quad (3.6)$$

$$2HO_2 + M \rightarrow H_2O_2 + O_2 + M \quad (3.7)$$

As the process of reaction indicates, the decomposition is strongly dependent on the available surface area where the peroxide molecule can interact with silver. The promotion of catalytic decomposition seems to be directly related to the exposed surface of the catalyst, suggesting a focus on designs that maximize surface area. The microchannel approach endeavors to increase

available surface area, but empirical results will indicate the validity of this method versus the surface area provided by the mesh catalyst approach.

2.2.2 Catalyst Bed Analysis and Sizing

An exhaustive exploration of the literature revealed little in way of a reliable method to correlate the volume flow rate of hydrogen peroxide to the relative surface area or length of a catalyst bed. The majority of previous applications reported using scaling models from functional catalyst rockets or determining the proper length entirely through empirical experimentation. In order to obtain an initial order of magnitude for the optimal length of this particular catalyst bed (the length at which it completely decomposes hydrogen peroxide into water and oxygen), a similar, blended approach was followed. Values from a MEMS scale thruster that used a microchannel catalyst bed approach were used to scale up to the estimated size required to fit in a picosatellite propulsion system. [Hitt and Zhou, 2003]. The primary value for this calculation is based on the thruster specific value of G, or density times velocity. The recorded values for a MEMS device were estimated to fully decompose hydrogen peroxide and were applied to obtain the estimated length L_{app} for this particular application.

$$G_{MEMS} = 800 \frac{kg}{s*m^2} \tag{3.8}$$

$$L_{MEMS} = 150 \times 10^{-6}\, m \tag{3.9}$$

$$G_{MEMS} = \rho * v = 65330 \frac{kg}{s*m^2} \tag{3.10}$$

$$\frac{\boldsymbol{G_{MEMS}}}{\boldsymbol{L_{MEMS}}} = \frac{\boldsymbol{800 \frac{kg}{s*m^2}}}{\boldsymbol{150E{-}6\ m}} = \frac{\boldsymbol{G_{App}}}{\boldsymbol{L_{App}}} \tag{3.11}$$

$$L_{app} = 1.2\ cm \tag{3.12}$$

Similarly, the concept of 'critical residence time' was borrowed from a large scale Air Force rocket that utilized a mesh catalyst [Thomas, 1998]. This calculation is focused on estimating a critical residence time, or the time requirement for hydrogen peroxide to be in contact with silver to be fully decomposed. This is an oversimplification, but provides a rough starting estimate. Using values from the selected configuration, and the estimated critical residence value (t_r) of .53 seconds, the following length was derived.

$$m' = .776 \frac{kg}{s} \tag{3.13}$$

$$A = 3.16 \times 10^{-5} m^2 \tag{3.14}$$

$$\rho = 1390 \frac{kg}{m^3} \tag{3.15}$$

$$\rho = v = \frac{m'}{A\rho} = .0177 \frac{m}{s} \tag{3.16}$$

$$L = v * t_r = .9\ cm \tag{3.17}$$

The initial catalyst bed size was set at 2 cm. This provided a base length for which to continue designing the system.

2.2.3 Work to Develop an Analytical Model

Throughout the process of developing this hydrogen peroxide thruster, a precise and reliable model for estimating the required catalyst bed length was quickly identified as a potentially useful tool. An analytical model was designed to achieve this, based on the work by Hitt and Zhou [2003] from the University of Vermont. This approach approximates the decomposition of peroxide to occur in five distinct regions, represented in Figure 16.

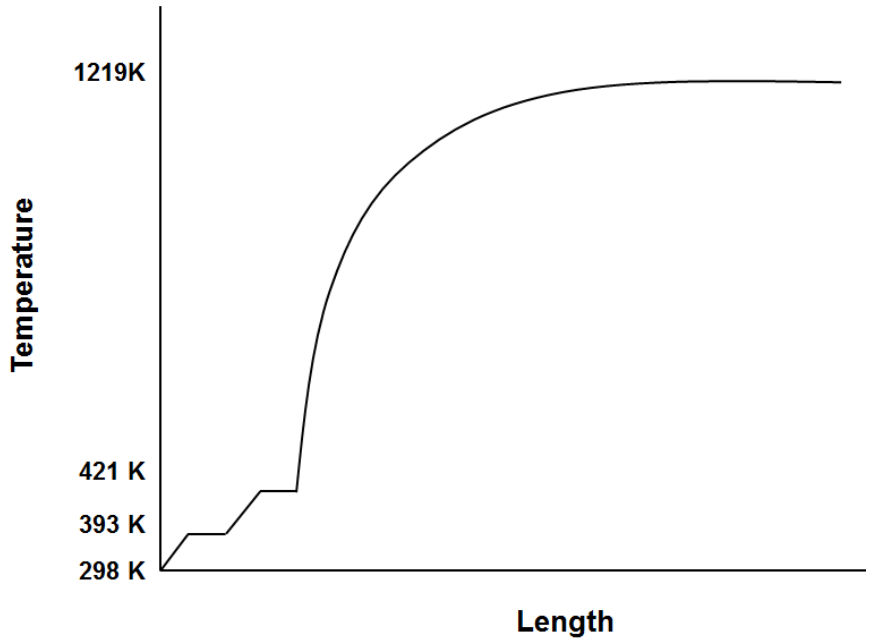

Figure 16. The decomposition process can be divided into five distinct sub-regions, based on temperature, for the purpose of deriving an analytical model based on energy conservation.

These are divided into Stage I: Heating of Bulk Liquid, Stage II: Evaporation of Water, Stage III: Heating of Hydrogen Peroxide Liquid, Stave IV: Evaporation of Hydrogen Peroxide, and Stage V: Bulk Decomposition of Hydrogen Peroxide. Two separate approaches were taken to use these assumptions to create a reliable model. The first used the approach below focused on energy conservation and specific heat (Eq. 3.18 and 3.19). The result of this approach can be seen in *Appendix H: MatLab Code* through the MATLAB script that was developed.

$$\Delta H = C_p \Delta T \tag{3.18}$$

$$\Delta H^0 = \Sigma[n_j \Delta H_j^0]_{products} - \Sigma[n_j \Delta H_j^0]_{react} \tag{3.19}$$

$$\frac{\Delta H^0}{mole} = 54.14\ KJ \tag{3.20}$$

$$k = A\, e^{\frac{-E}{RT}} \tag{3.21}$$

Eq. 3.21 is known as the Arrhenius equation and estimates a reaction rate. Values for the activation energy (E), and the pre-exponential factor (A) were those of the reaction rates with iron, which is estimated to be similar [Hitt and Zhou, 2003]. Where:

$$A = 8E10\ \frac{1}{s} \tag{3.22}$$

$$E\ = 13100\ \frac{cal}{mole} \tag{3.23}$$

Once the reaction rate was determined, the change in concentration could be ascertained at the starting concentration of each stage. The general approach, expanded in Eq. 3.24 allows a rough estimate of time, from which a length can then be found with flow velocity.

$$C_a\ \rightarrow\ \frac{dC_a}{dt}\ \rightarrow\ C_b\ \rightarrow t_a \tag{3.24}$$

Additionally, a more complete estimate using a differential equation solver in Python was also worked on with MIT LL personnel. This approach yielded similar results, but focuses on solving the complete system of conservation equations [Hitt and Zhou, 2003].

$$\frac{d(\bar{p}u)}{dx} = 0 \tag{3.25}$$

$$\frac{d(\bar{p}u^2)}{dx} = -\frac{dp}{dx} \tag{3.26}$$

$$\frac{d(\bar{p}C_p uT)}{dx} = Q\omega - \alpha[T(x) - T_\infty] \tag{3.27}$$

$$\frac{d(\bar{p}uY_i)}{dx} = -W_i\omega \qquad (i = 1,2,3) \tag{3.28}$$

The problem encountered in both models hinged on the reaction rate. For the numerical method, a constant reaction rate was assumed at 1 x $10^8\ \frac{1}{s}$. This reaction rate drives Stage V, which, in turn, is the dominant factor for catalyst bed length. Figure 17 exhibits the inherent difficulty in choosing an accurate reaction rate from extrapolated data in the literature.

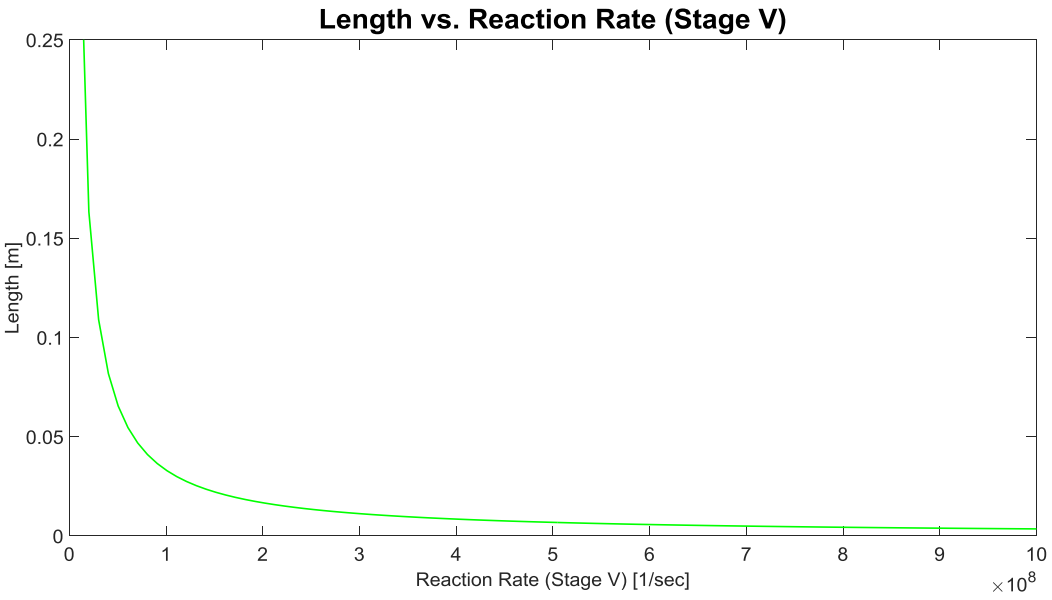

Figure 17. The length of the catalyst bed varies greatly with the associated reaction rate of the catalyst and hydrogen peroxide.

A slight deviation in reaction rate can drastically alter the estimated length. Future work will need to be conducted to precisely identify the reaction rate values for hydrogen peroxide and silver in order to complete this analytical model.

2.2.4 Activating the Catalyst

Untreated pure silver proved to be a poor catalyst upon immediate exposure. Turning to the literature, several reports indicated exposing the silver to nitric acid and heating to 900 K as an appropriate means of activation. No oven was available that could reach the prescribed temperature, leaving us to experiment with solely nitric acid. A one minute exposure to the nitric acid however, only provided a slightly greater reaction. With the help of a MIT LL chemist, a new procedure was adopted.

The silver was placed in a hydrochloric acid bath for 30 seconds. It was removed and immediately rinsed with de-ionized water and dried. The catalyst bed was then exposed to 35

weight percent hydrogen peroxide in for 2 – 3 minutes, until the reaction is immediate and violent upon contact with peroxide. It may take several minutes for the reaction rate to speed up to a desirable level.

The theorized method of this activation procedure is related to the surface area of the silver. The hydrochloric acid acts to remove impurities from the surface, while increasing the surface roughness, and consequently surface area. The conditioning period in the hydrogen peroxide acts to remove the surface layer of the silver, creating an oxide and speeding up the rate of reaction. Further studies into this phenomenon will need to be conducted, and alternate activation procedures should be explored.

2.2.5 Catalyst Bed Fabrication

The catalyst bed fabrication was originally centered on machining the microchannels through a solid rod of pure silver. This proved difficult in terms of fabrication on multiple accounts. The diameter of the required holes was beyond the limit of a traditional drill bit, and the effectiveness of electrical discharge machining was negated beyond lengths of a few millimeters.

This led to a redesign of the catalyst bed in order to account for ease of machinability. The resulting configuration proved tremendously easy to assemble, while retaining the reaction surface area of the previous design and maintaining strong mechanical properties. This new catalyst was built by press fitting a bundle of 1.45 mm diameter silver tubes into a bored out, 6.35 mm diameter silver rod. This provides a seat for sealing around the outside edge with increased surface area through the interior of the catalyst bed. The design was assembled in house and proved remarkably versatile in quickly manufacturing a variety of catalyst bed lengths.

2.3 Nozzle Design

The CanSat volume and performance requirements for the propulsion system both drive and constrain the possible for nozzle configurations. These requirements were arrived at through collaboration with MIT LL and research of potential picosatellite missions. Maneuver acceleration must be between 0.05 m/s^2, and 0.25 m/s^2. The resulting slew rate of the craft can range from 10°/s to 300°/s, and the pointing accuracy needs be less than 1°.

2.3.1 Nozzle Theory

The operating parameters of nozzle design are heavily dependent on suitable assumptions from the ideal rocket theory as well as isentropic expansion of flow. The ideal rocket theory has 11 postulates that describe the concept of an ideal rocket propulsion system. Because basic thermodynamic principles can be expressed as simple mathematical relationships, these assumptions permit derivation of a simple quasi-one-dimensional flow. However, in reference to postulate eight which states that "all exhaust gases leaving the rocket have an axially directed velocity", divergence losses are discounted because of the use of a conical nozzle exit with an 18° half angle. Also due to the micro-thruster size, energy losses due to heat escaping through the walls of the rocket might lead to decreased rocket performance (at least 2%). Therefore coefficients of loss were established to account for this phenomenon. Primary equations in this section were pulled from the eighth edition of *Rocket Propulsion Elements* by Biblarz and Sutton [2010].

2.3.2 Nozzle Configurations

The major operating parameters for the design of a nozzle to flow decomposed hydrogen peroxide include the area expansion ratio and the ratio of specific heats. From the selection of the hydrogen peroxide propellant at the concentration of 98 weight percent, the ratio of specific

heats for 98% the products of decomposed hydrogen peroxide is 1.251 [Ventura, 2001]. Down selection of the area expansion ratio focused on minimizing the length of the nozzle for use in a volume constrained environment. Iterations were performed from an initial value of 25 until the final value of 10 was selected for the axial nozzle. Also, research into previously developed thrusters indicated an appropriate chamber pressure of 100 psi. This dictated the mass flow rate per cross sectional area at the entrance. A summary of the key assumptions can be found in Table 8.

Table 8. Several important design assumptions were reached in order to begin design. These stemmed from research and practical knowledge and are summarized here.

Specific Heat Ratio (k)	1.251
Area Expansion Ratio (AER)	10
Inlet Pressure (P_1)	100 psi (689476 Pa)
Inlet Temperature (T_1)	1219 K
Wet Mass (m_o)	1.025 kg
Molecular mass (MM)	26.48 kg/kmol
Mach at Throat (M_t)	1
Conical Half Angle (α)	18°

Hydrogen peroxide's adiabatic flame temperature is 1219 Kelvin and is assumed to be the inlet temperature of the nozzle. Using the inlet temperature (T_1) and the ratio of specific heats (k) the temperature at the throat of the nozzle ($T_{t)}$ is given by

$$T_t = \frac{2T_1}{k+1} = 1083\ K \tag{3.29}$$

Next, the Mach number at the exit of the nozzle (M_2) is determined by k and area expansion ratio (AER) as

$$AER = \frac{1}{M_2}\left(\frac{1+\frac{k-1}{2}M_2^2}{\frac{k+1}{2}}\right)^{\frac{k+1}{2(k-1)}} \tag{3.30}$$

$$M_2 = 3.4294 \tag{3.31}$$

The following isentropic expressions are used:

$$T_o = T_t\left(1 + \frac{k-1}{2}M_t^2\right) \tag{3.32}$$

$$T_o = 1219\ K \tag{3.33}$$

$$T_2 = \frac{T_o}{1+\frac{k-1}{2}M_2^2} \tag{3.34}$$

$$T_2 = 492\ K \tag{3.35}$$

In order to use Eq. 3.34, Eq. 3.32 must first solved to determine if stagnation temperature (T_0) is equal to T_t, an assumption in most applications. T_0 is derived using T_t, k, and M_t from Eq. 3.32, then T_2 is derived using T_0, k, and M_2 .

Utilizing the following relations, the exit velocity (V_2) and exit pressure (P_2) are obtained

$$V_2 = M_2\sqrt{kRT_2} = 1508\frac{m}{s} \tag{3.36}$$

$$P_2 = P_1\left(\frac{T_2}{T_1}\right)^{\frac{k}{k-1}} = 7518\ Pa \tag{3.37}$$

To achieve the goal of 0.25 g's of acceleration, a total thrust of 2.5 N is needed, as shown by

$$F = ma,\ m = 1.025\ kg,\ a = 0.25\frac{m}{s^2} \tag{3.38}$$

$$F_{total} = 1.025\ kg\ \left(0.25 * 9.81\frac{m}{s^2}\right) =\ 2.5\ N \tag{3.39}$$

Since there are two thrusters on each axis of motion, the total thrust is divided in half,

$$F = \frac{2.5}{2} N = 1.25\ N \tag{3.40}$$

The cross sectional area at the throat of the nozzle (A_t) can be calculated using Eq. 3.43 and the given thrust$F$, P_1, T_1, k, specific gas constant (R_s), V_2, and P_2. The universal gas constant is given by the ideal gas constant and molecular mass $(MM) R = 8.3144621 \frac{J}{mol*K}$

$$(3.41) R_s = \frac{R}{MM} = 314 \frac{m^2}{K*s^2} \tag{3.42}$$

The throat area is then

$$A_t = \frac{F}{\left(\frac{P_1}{\sqrt{T_1}}\sqrt{\frac{k}{R_S}\left(\frac{2}{k+1}\right)^{\frac{k+1}{k-1}}}\right)V_2 + 10P_2} = 1.058\ mm^2 \tag{3.43}$$

The nozzle exit area (A_2) is given in terms of the known AER and A_t as

$$AER = \frac{A_2}{A_t}, \quad A_2 = 10.58\ mm^2 \tag{3.44}$$

Using isentropic data tables for compressible fluids [Ave, 2006], cross sectional area at the nozzle inlet is easily attainable

$$\frac{A_1}{A_t} = 11.72,\ A_1 = 12.40\ mm^2 \tag{3.45}$$

The diameters at the inlet (D_1), throat (D_t), and exit (D_2), are derived from

$$A_x = \frac{\pi {D_x}^2}{4},\ D_x = \sqrt{\frac{4A_x}{\pi}} \tag{3.46}$$

$$D_1 = \sqrt{\frac{4A_1}{\pi}} = 3.9733\ mm \tag{3.47}$$

$$D_t = \sqrt{\frac{4A_t}{\pi}} = 1.1606\ mm \tag{3.48}$$

$$D_2 = \sqrt{\frac{4A_2}{\pi}} = 3.6702\ mm \tag{3.49}$$

The shape of the nozzle exit is conical as shown in Figure 18. The length of the cone is influenced by the half angle, which is the angle between the nozzle exit wall and centerline of the cone, lengthwise.

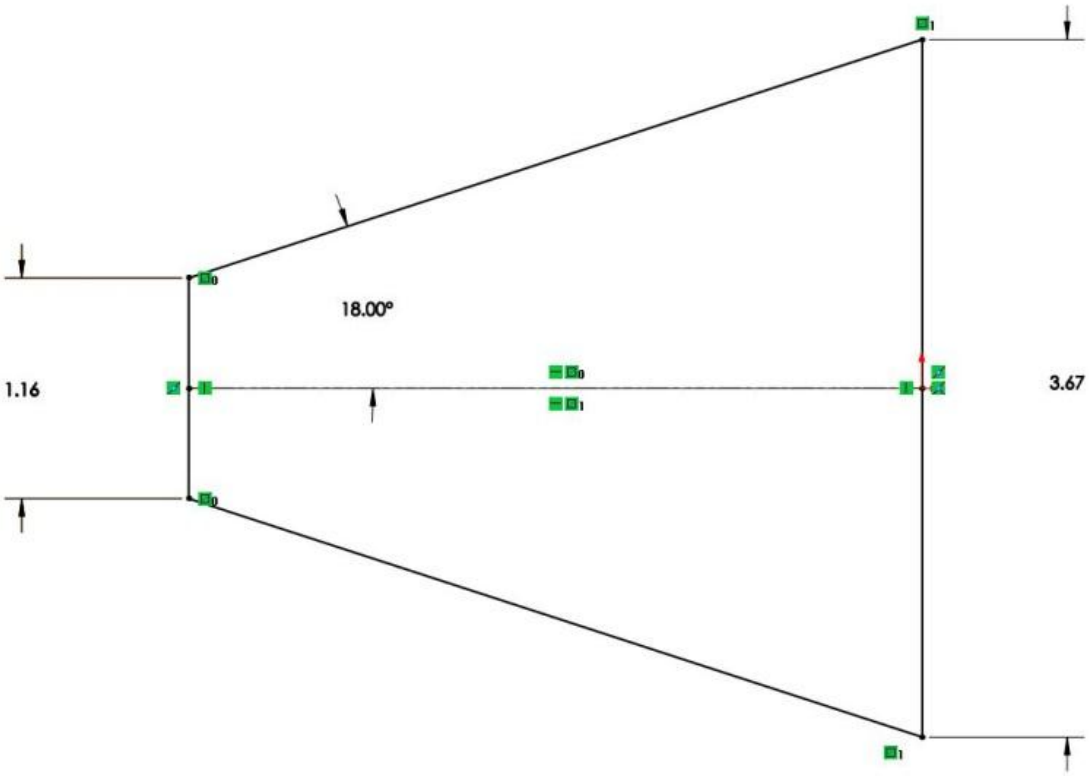

Figure 18. A conical nozzle was chosen to simplify the machining process.

For solving the length of the cone Eq. 3.50 is used.

$$L = \frac{\frac{D_2 - D_t}{2}}{\tan\left(\alpha \times \frac{\pi}{180}\right)} = 3.862\ mm \tag{3.50}$$

The final nozzle design configuration is presented in Table 9:

Table 9. A complete summary of the nozzle design was calculated in order to achieve the desired accelerations for the satellite.

Specific Heat Ratio (k)	1.251
Area Expansion Ratio (AER)	10
Inlet Pressure (P_1)	100 psi (689,476 Pa)
Inlet Temperature (T_1)	1,219 K
Wet Mass (m_o)	1.025 kg
Molecular mass (MM)	26.48 kg/kmol
Mach at Throat (M_t)	1
Conical Half Angle (α)	18°
Throat Temperature (T_t)	1,083 K
Exit Mach (M_2)	3.4294
Stagnation Temperature (T_o)	1,219 K
Exit Temperature (T_2)	492 K
Exit Velocity (V_2)	1,508 m/s
Exit Pressure (P_2)	1.09 psi (7,518 Pa)
Thrust (F)	1.25 N
Throat Area (A_t)	1.058 mm^2
Exit Area (A_2)	10.58 mm^2
Inlet Area (A_1)	12.40 mm^2
Exit Diameter (D_2)	3.6702 mm
Throat Diameter (D_t)	1.1606 mm
Inlet Diameter (D_1)	3.9733 mm
Cone Length	3.862 mm

2.3.3 Thruster and Catalyst Block Fabrication

The thrust block, shown in Figure 19, is composed of 316 stainless steel, holds the catalyst bed and nozzle, as well as connections for a thermocouple and pressure sensor for measuring the pressure and temperature of the decomposed hydrogen peroxide immediately before it enters the nozzle. Specific drawings can be found in *Appendix I: Drawings*. The primary purpose of the thrust block structure is to provide a secure seat for the catalyst bed, which will lead into a chamber attached to the nozzle. A 90° configuration was adopted due to

space constraints in the fume hood used for testing. Three bolts mount this block to the thrust stand and the flow control valve connects to a tee fitting that attaches directly into the block. Using the preliminary estimates from scaling, this thruster block was designed to specifically accept the 2 cm long catalyst bed.

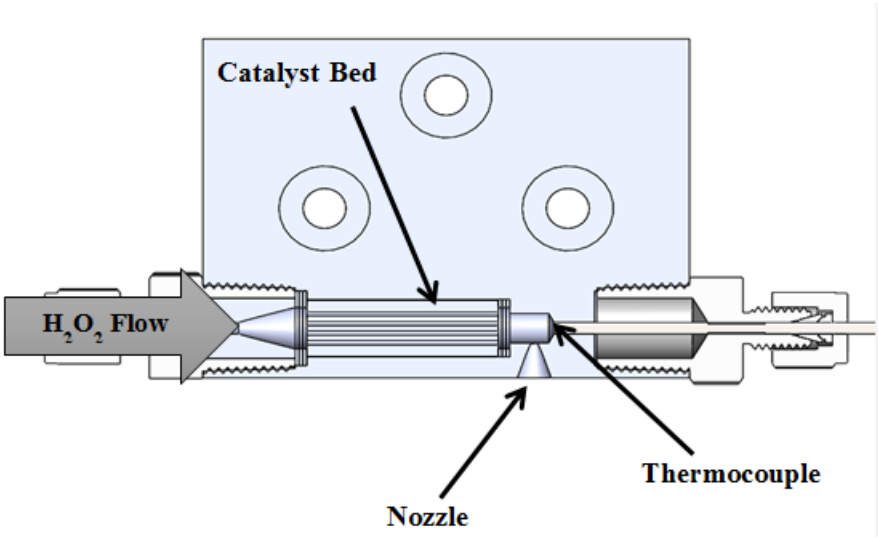

Figure 19. The experimental thrust block attempted to recreate an arrangement similar to that expected in the objective design.

Also made of 316 stainless steel, a derivative of this design was created to house the catalyst beds for testing and can also be found in *Appendix I: Drawings*. The objective of this block was similar, though safety was a much more pressing issue due to the decomposed hydrogen peroxide that was expected to flow through. The internal structure of the catalyst block resembles that of the thrust block. Instead of the chamber releasing into the nozzle, it is expanded into a much larger pipe, at which point it is drained through a ¾ inch pipe into a beaker to analyze decomposition. In order to use the same catalyst block to test a variety of different lengths, a holding adapter shim was made to accept each length. The inside of the catalyst bed was sealed with custom made copper gaskets, and a secondary gasket seal was used at entrance to the block.

3 Ground Support Equipment

This chapter addresses the associated equipment and devices that needed to be fabricated or procured in order to complete the setup. The method of measuring and characterizing the system is also discussed.

3.1 Thrust Stand Concept and Design

The most vital component of our ground support equipment (GSE) is the thrust stand, which supports the thruster system and is capable of measuring the force exerted by the thruster. Initially, research was conducted on a variety of thrust stand concepts from papers where other teams had performed similar thrust tests. Goals for the thrust stand were for it to be simple and easy to manufacture in-house, while also easy to calibrate and having relatively precise thrust measurement capability. The stand had to be able to measure expected thrust range (<1N) with an accuracy of +/- 0.05 N. The following concepts were carefully explored for use.

3.1.1 Inverted Pendulum Thrust Stand

One of the most widely used thrust stands for precise measurements is an inverted pendulum thrust stand. The basic inverted pendulum stand design consists of a vertically oriented rotating arm with the thruster on top and a spring or flexure to provide a reaction force (Figure 17). The thrust is measured through calculation from the data measured with a Linear Variable Displacement Transducer (LVDT) mounted between the rotating arm and a fixed wall. NASA's Thomas Haag [1989] used this thrust stand design for measuring thrust from a high powered electric propulsion device.

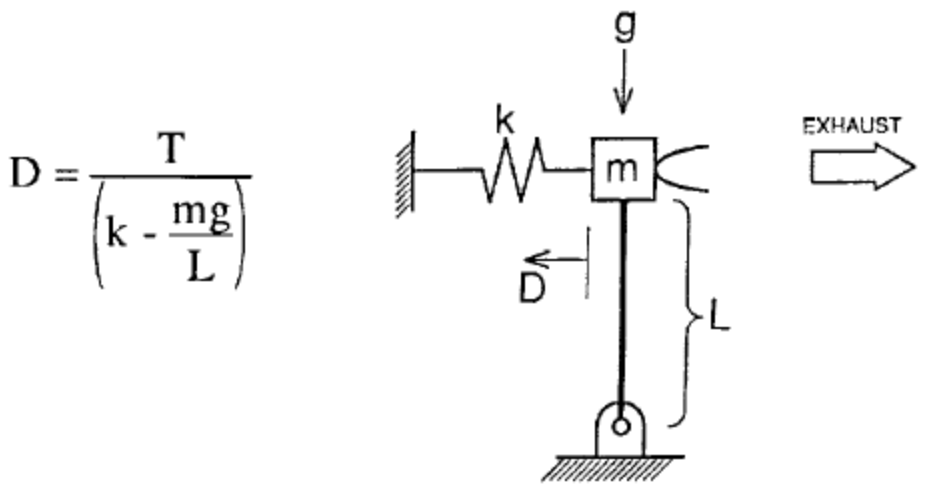

Figure 20. A schematic illustrates the functionality of an inverted pendulum thrust stand [Haag, 1989].

3.1.2 Suspended Plate Thrust Stand

Another common design is a suspended plate thrust stand. This measurement device consists of a thin plate suspended by lines connected from a base to the corners of a rectangular plate. The entire system is placed on the plate, reducing the possibility of interference from wires and tubing. The thrust is measured from the output of a strain gage placed on a thin copper strip which connects the suspended plate to a rigid structure.

3.1.3 Torsional Thrust Stand

Eventually a torsional thrust stand was decided on as the most viable stand for testing the thruster. A torsional thrust stand was used by Haag [1996] to measure the output of a pulsed plasma thruster (PPT) and is shown in Figure 21. The typical torsional thrust stand measures thrust by measuring the displacement of an arm connected to a shaft which pivots about the vertical axis.

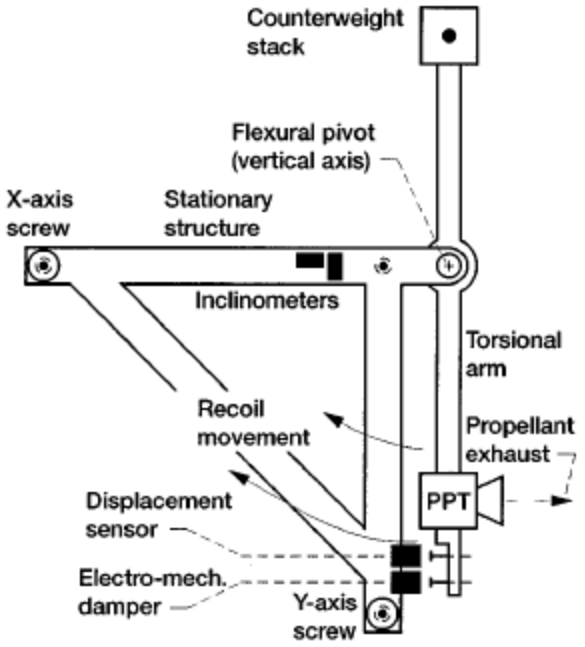

Figure 21. A schematic illustrates the functionality of a PPT torsional thrust stand [Haag, 1989].

3.1.4 Torsional Thrust Stand Fabrication

The torsional thrust stand was settled on because of its conceptual simplicity and ease of fabrication. However, instead of relating the thrust directly to a displacement sensor, a torque transducer was installed at the base of the shaft. An Omega TQ202 reaction torque sensor with a 0-0.7 N-m range was chosen as the torque sensor. As expected thrust is no more than 1 N and the our nozzle outlet is located 8.1" (.21 m) from the rotational axis, the expected torque measurements fall at ~0.3 N, well within the range of the sensor.

The thrust stand is mounted on three adjustable feet for precise leveling. The arm of the thrust stand is 18 inches long, extending from the center axis 9 inches in either direction. The center shaft is 3.5" tall and is connected to the torque sensor on the bottom and a ball bearing on the top. The thruster block, containing nozzle and catalyst bed, is located on the right of the arm,

while a counterweight to offset the system components is located on the left side of the arm Figure 22 and Figure 23 show the SolidWorks model that was designed to meet the requirement.

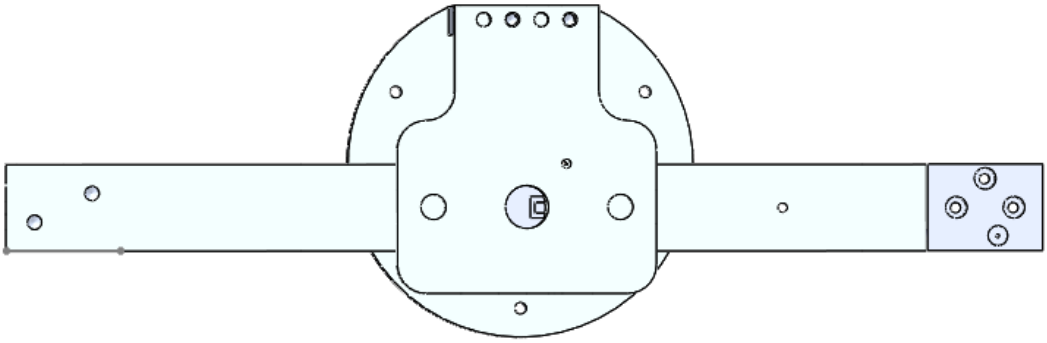

Figure 22. A top view of the torsional thrust stand.

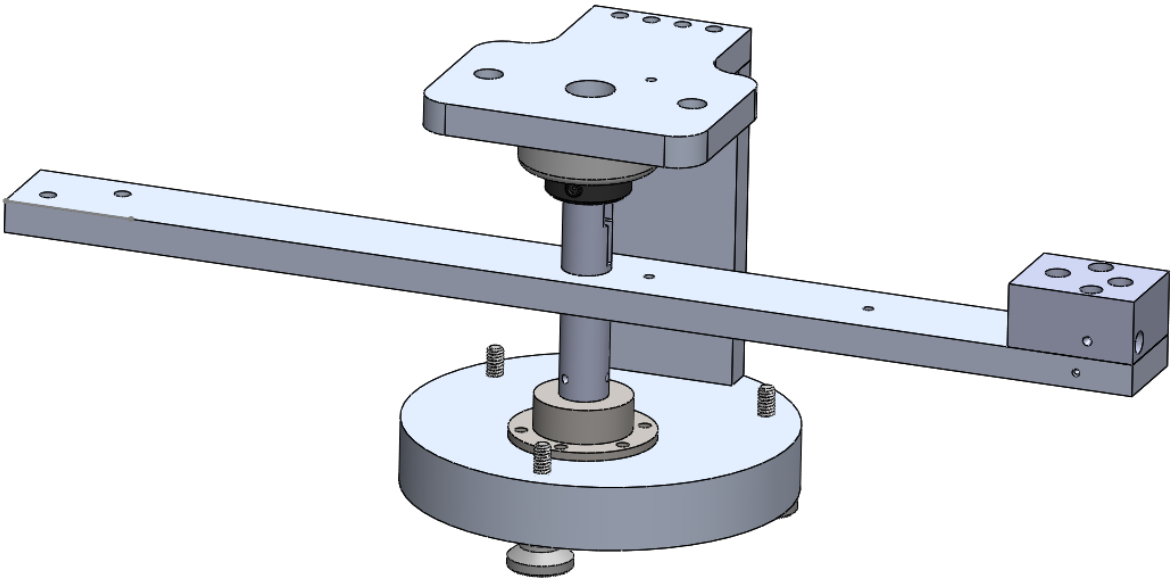

Figure 23. An isometric view of the thrust stand design.

The thrust stand consists of six custom designed and machined components. The base of the thrust stand was manufactured out of 1 inch thick 304 stainless steel. It contains holes for

mounting the torque sensor, levelling feet, and neck (Figure 24). The neck is mounted onto the base and the top via alignment pins and bolts (Figure 25). It was manufactured out of ½" 6061 aluminum.

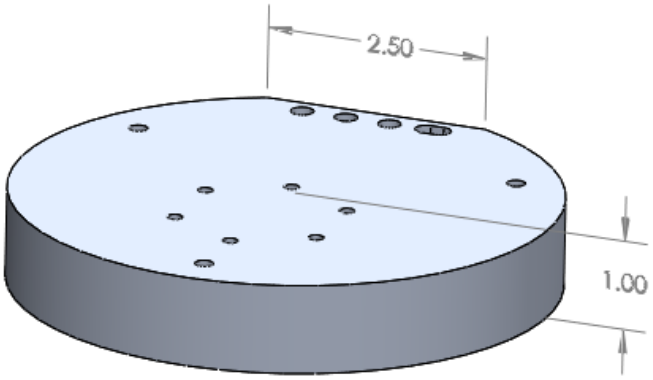

Figure 24. An isometric view of the thrust stand base.

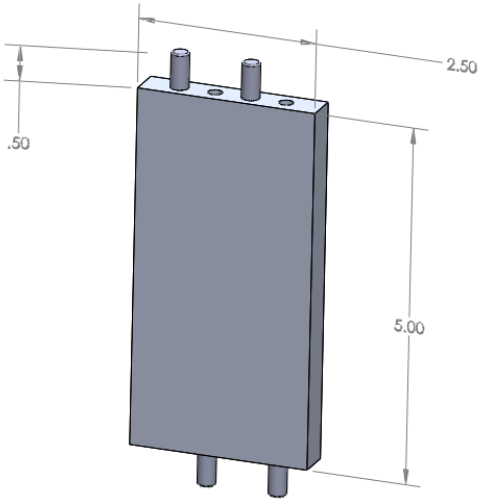

Figure 25. The neck of the thrust stand was designed for a precise fit.

The top of the thrust stand has connections for the ball bearing and the neck. It is also made out of 6061 aluminum. The shaft, made from a ¾" rod of 304 stainless steel, is connected to the ball bearing via a set screw, and it is press fit into the arm (Figure 26). The shaft has three set screws on the bottom to connect to the torque sensor (Figure 27).

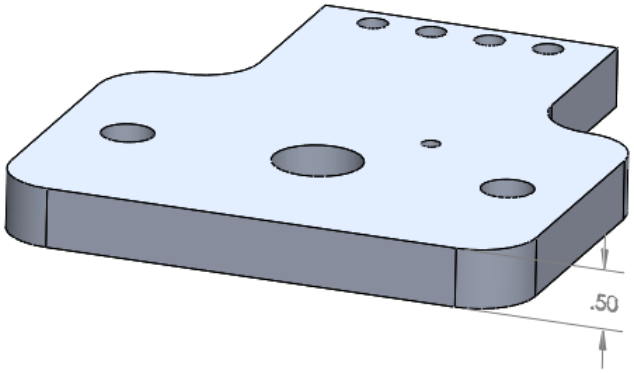

Figure 26. An isometric view of the top of the thrust stand. A bearing attaches to this piece, allowing for free rotation of the shaft

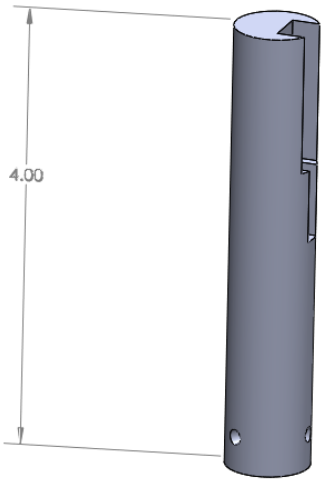

Figure 27. In addition to providing the center axis for the torque arm, a slot in the top of the shaft allows for tubing and wiring to be fed through the center. This attempts to negate irregularities in thrust measurement.

The arm of the thrust stand is made out of aluminum, and is 18 inches long, 1.5 inches wide and 0.5" thick. It contains connections for the thrust block on one end and for a counterweight on the other end (Figure 28). The estimated the counterweight value of 1.38 lb was derived using Soldiworks® center of mass analysis.

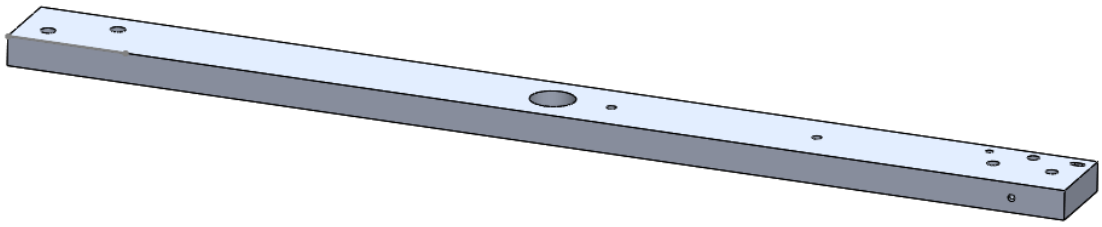

Figure 28. An isometric view of the arm and connection points.

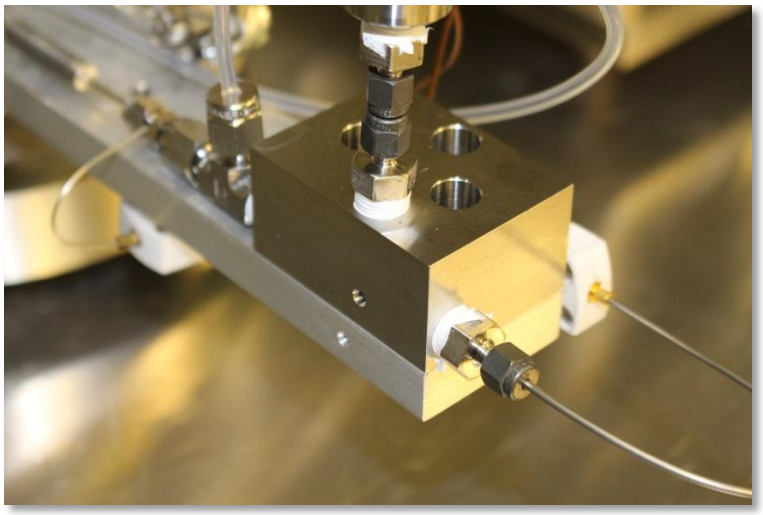

Figure 29. Installation of the thrust block onto the thrust stand proved easy and robust.

3.2 Experiment Setup

The test setup consists of the thrust stand, the required flow equipment and control and data collection devices. Through integration of each of these components, a complete test bed was assembled inside a contained fume hood.

3.2.1 Flow Equipment

The method for pressurizing the system involves a Chemyx Nexus 6000 syringe pump, capable of applying a nominal linear force of 450 lbs, and leak proof up to 700 psi. The pump is fitted with a 200 mL stainless steel syringe, also from Chemyx, The pump is controlled via an on-pump screen and buttons or with commands in Hyperterminal over an RS232 connection. The pump is set by determining the amount of liquid and the rate to infuse or withdraw; for example, it could be set to pump 100 mL of water into the system at a rate of 175 mL/s. This method is not ideal, as there is no response to pressure, and a constant system pressure is nearly impossible to obtain. Considerations were made to implement a pressure feedback loop via RS232 communication to the pump, but due to time constraints, it was decided to operate it manually.

Figure 30. A Nexus 6000 syringe pump was used to contain and pressurize the propellant.

The control valve chosen for the system is from the Lee Company's IEPA series, specifically the IEPA1221141H solenoid valve, indicated in Figure 31. This valve can operate in the proposed pressure range and is compatible with hydrogen peroxide. The reaction time of the valve is very quick at 1.5 ms, favorable for use in the objective system. As seen in the diagram below, the valve itself is just over one inch long and has a diameter of ¼". The wetted materials

in the valve are 316 Stainless Steel, FKM and ChromeCore®18. Based on materials research and compatibility testing, it was found that all the materials were safe for use with hydrogen peroxide.

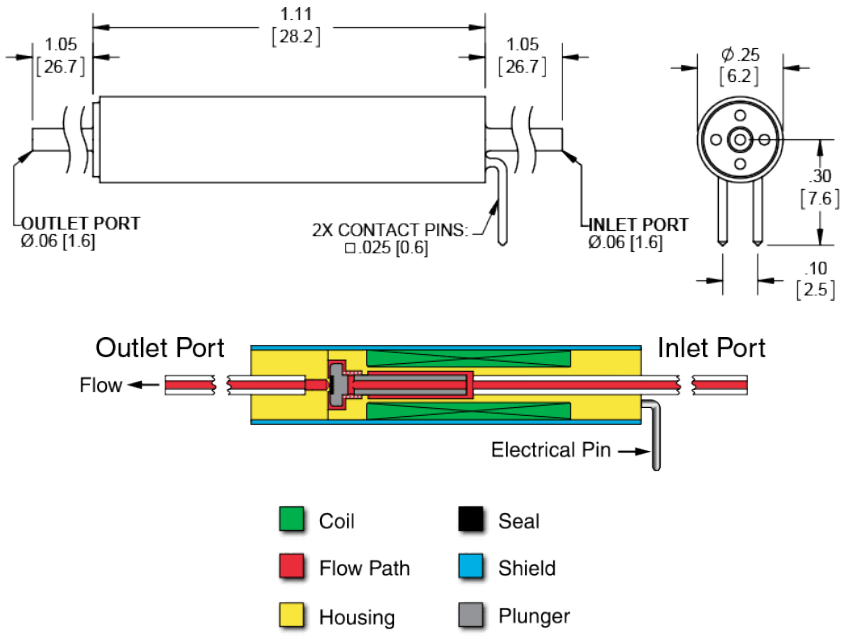

Part No.	SEAL MATERIAL[1]	SPIKE Voltage (vdc)	HOLD Voltage (vdc)	Power @ HOLDing VOLTAGE[2] (W)	Max. SPIKE DURATION[3] (ms)	MAx. OPERATING PRESSURE psig (bar)	MAX. AMBIENT TEMPERATURE °F (°C)	FLOW[4] Lohms (Cv)
IEPA1221141H	FKM	12	1.6	0.25	2	800 (55)	275 (135)	4100 (.005)

Figure 31. A Lee IEP solenoid valve was selected to control flow to the thrust block. Image courtesy of The Lee Company.

In order for the Lee valve to be pulsed, a driver circuit needed to be created. Based on the circuit design from the manufacturer, circuits were made according to the diagram in Figure 32. Taking inputs of 12 V, 5 V, and 1.6 V and a control signal of high value of 5 V, the circuit outputs a 12V spike and then holds at 1.6 V to keep the valve open until the control signal is low. The control signal vs. output diagram is also shown in Figure 32.

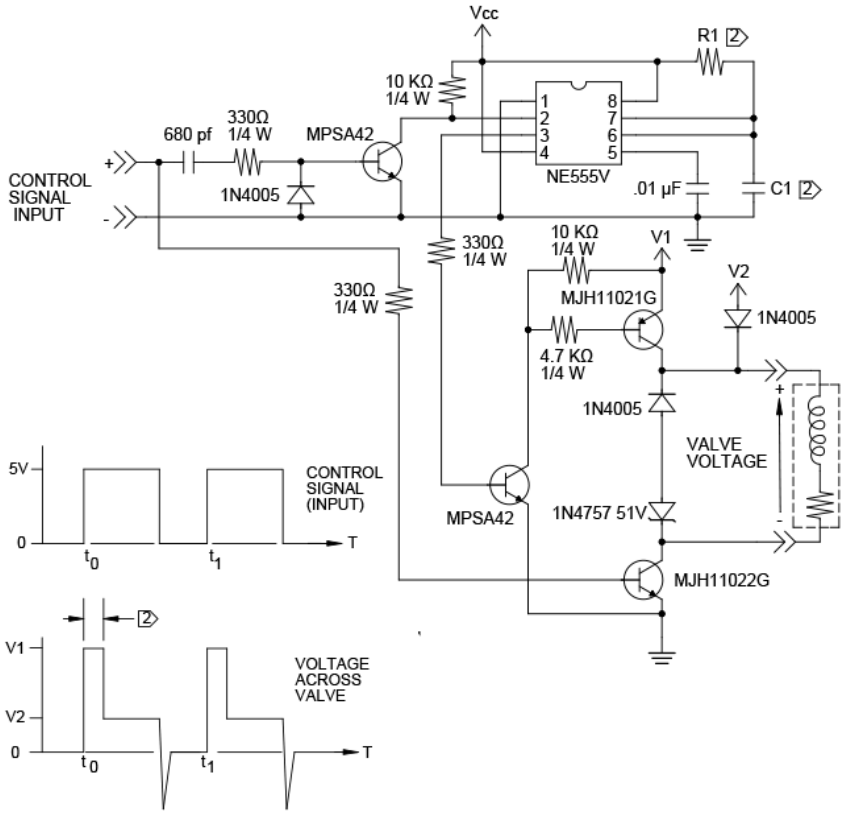

Figure 32: Valve Driver Circuit Diagram

The system has a single relief valve, set at a cracking pressure of 200 psi. It leads to a stainless steel bucket filled with water, for immediate dilution of hydrogen peroxide. This relief valve is a Swagelok SS-RL3M4-F4 relief valve, made of stainless steel and lubricated with a lubricant compatible with hydrogen peroxide (Krytox). A second Lee valve with a manual control switch acts as a relief valve just prior to the thrust block. This also leads into the water-filled stainless steel bucket.

The tubing used is 1/8" OD 316 Stainless Steel and Teflon PFA. The Teflon PFA tubing is rated for pressures up to 410 psi, and the stainless steel tubing is rated for pressures to 5000 psi. The fittings are all 316 Stainless Steel Yor-Lok compression fittings from McMaster-Carr.

3.2.2 Sensors and Data Collection Equipment

The sensors in our system include a torque sensor, three thermocouples and two pressure sensors. The torque sensor is a 0-0.2 N-m TQ202 reaction torque sensor from Omega Engineering. Testing initially started with a 0-0.7 N-m torque sensor, but the 0-0.7 sensor failed and was replaced it with the backup 0-0.2 N-m sensor. This sensor takes a 10 V excitation and outputs 0-10 mV with an accuracy of +/- 0.2% FSO.

The three thermocouples are standard type K high temperature thermocouples with stainless steel sheathing from Omega Engineering. The system contains two pressure sensors, one in the main line between the relief valve and the control valve and a second connected to the thrust block which measures the chamber pressure. The chamber pressure sensor is a USB output pressure sensor from Omega Engineering with a range of 0-5000 psia and an accuracy of +/-0.08% FSO. The other pressure sensor is an in-line pressure sensor from Setra, which has a range of 0-250 psia with an excitation of 10 V, output of 0-5 V and accuracy of +/-0.08% FSO.

The data collection system is the DaqBook 2020 with DaqView software. The DaqBook itself supports 14 thermocouple inputs and 16 differential voltage inputs and has a 220 kHz sample rate with 16 bit resolution. An independent wave form generator and separate power supplies for each sensor were set up as well. Using this setup enables viewing, logging, and saving of real time data in multiple file formats. All the sensors are connected to the DaqBook except for the USB output pressure sensor, which has its own simple data logging program.

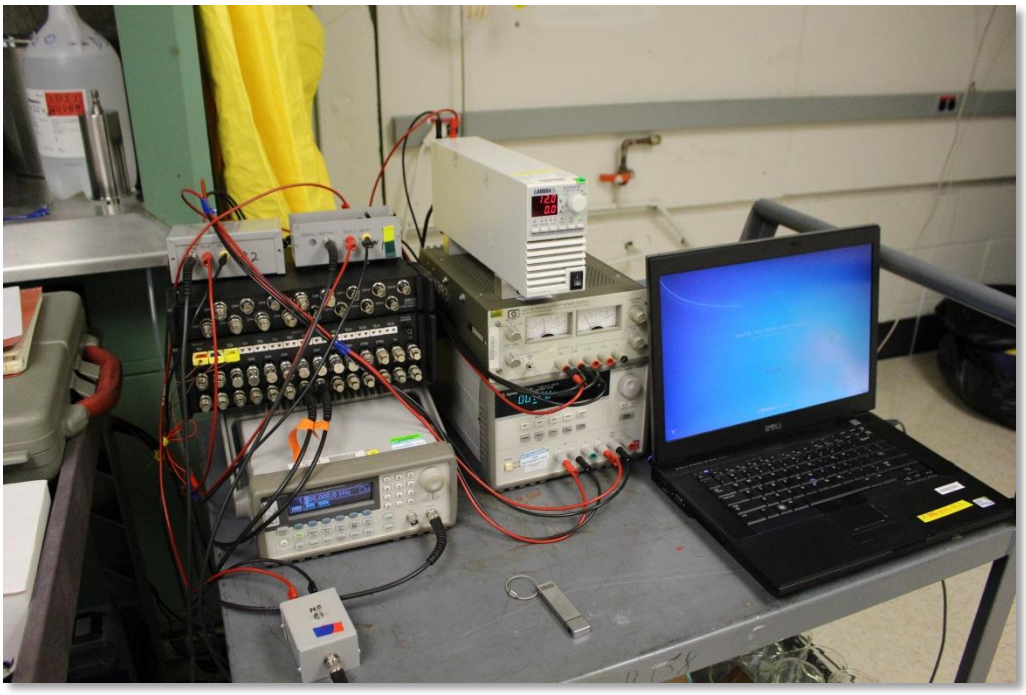

Figure 33. The electronic setup to control the valve was placed on a cart directly next to the test hood.

3.2.3 Material Compatibility

Hydrogen Peroxide, as an oxidizer, will react violently when in contact with organic substances and many inorganic substances. Before deeming any component safe to use in the system, research was conducted on its components and their reactivity to hydrogen peroxide. The main reference used for information on material compatibility was the FMC Bulletin No. 104: Materials of Construction for Equipment in use with Hydrogen Peroxide, 1966 revision. The FMC bulletin contains the results of material compatibility tests that FMC Corporation performed with 90% to 98% hydrogen peroxide and recommendations for compatible materials. A complete list of component material used in the system is summarized in Table 10.

Table 10. Due to the reactive nature of hydrogen peroxide, appropriate material was chosen for all wetted components.

Material	Component(s)	Rating (1 = low reactivity- 4 = high)
316/304 Stainless Steel	Fittings, Tube, Valves, Thrust Block, base of thrust stand	2 – recommended for Machined Parts
6061 Aluminum	Top plate, arm and neck of Thrust Stand	2 – Subject to corrosion
Teflon	Tubing, Lining for fume hood, O-rings	1 – Various uses
Viton	O-rings	2 – "O-rings", seals, bladders
Lexan	Blast Shield	2 – plastic lines, components

A few materials did not have any data on their compatibility with hydrogen peroxide, as this guide had been published in 1966 and no comprehensive source was found from after then. Accordingly, materials compatibility tests were performed with 30 weight percent peroxide which was on hand in Lincoln Laboratory's Microelectronics Laboratory. From the results of the compatibility tests, it was found that all of the questionable materials, the Chrome Core, PVC glove, FKM, Alumina and Pyro Putty samples are safe for use with hydrogen peroxide. The Pyro Putty did have a small reaction, but as it will be used after the major decomposition of hydrogen peroxide in the catalyst bed, there should not be any difficulties using it.

4 Test Results and Discussion

In this chapter, the series of preliminary and live tests conducted on the system are presented, analyzed, and discussed.

4.1 Proof Testing the System

Initial testing began with leak checking the system without the thrust block connected and following the procedures outlined in *Appendix D: Laboratory Protocols*. The system was first pressurized with nitrogen gas incrementally until the pressure sensor read ~115 psia. It sat for a few minutes, and was depressurized. After initially pressurizing the system, the cracking pressure of the relief valve was tested by pressurizing the system incrementally up to ~188 psia, where bubbling in the bucket the relief valve was connected to, was recorded, indicating that the valve had cracked. The pressure was then lowered, reseating the valve, and then the system was pressurized again, repeating this process three times.

After testing the cracking pressure of the relief valve, leak testing began. The system was pressurized with nitrogen gas to ~115 psia, and then the valve connecting to the nitrogen source was closed, isolating the system, while recording data. During the first test, a pressure loss of about 1 psi/min was recorded. To identify the leak, the system was sprayed with deionized water and bubbling was found at the leak. The leaking fitting was tightened, and testing proceeded, leaving the system pressurized and isolated for 2-3 hours.

After the second test, a small nitrogen loss was still apparent, forcing to the transition to a helium leak test to isolate the trouble spot. The helium test works by attaching a vacuum to the system and flowing helium over the fittings. The vacuum will pull in any helium and a spectrometer measures the presence of helium, signifying a leak. In this way, a faulty fitting was identified, which was subsequently eliminated from the system. Ultimately, a small leak

remained, but its average discharge was measured as a loss of 0.29 psi/hour (Figure 35). Further helium testing indicated a miniscule leak that would likely be too small for liquid to pass through. Pressurizing the system with water for several hours validated this assumption.

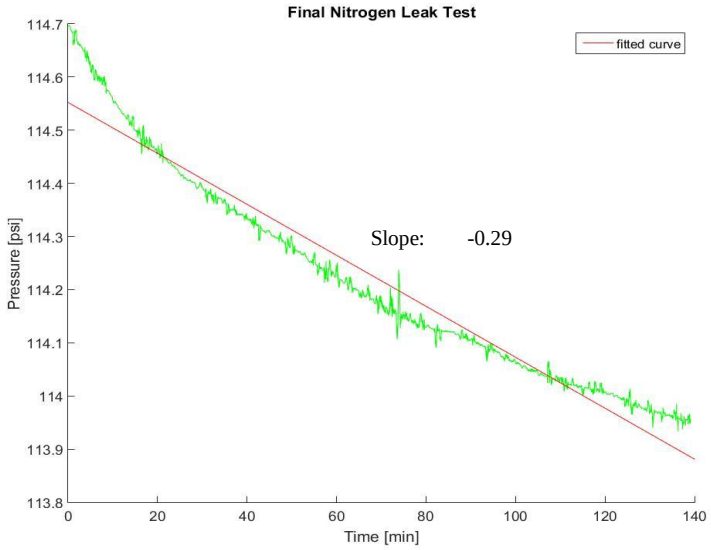

Figure 34. A test of the system with nitrogen gas indicated initial leaks in the system. Changes were made to provide a leak free system for hydrogen peroxide use.

4.1.1 Sensor Calibration

Before starting any thrust tests, the torque sensor was calibrated by placing a force gauge on the nozzle and applying a known force while reading the output voltage of the torque sensor; the setup is picture in Figure 35. Since the relationship between output voltage and applied torque to the torque sensor is linear, and the moment arm is a static length, the

Figure 35. An accurate force gauge was used to provide a known force in order to calibrate the torque sensor.

calibration curve for the equipment was identified (Figure 36 and Figure 37) and then plugged into the DAQView software to record our data in newtons. The torque sensor was calibrated via force, and not torque, so a direct thrust measurement was obtained.

The sequence used for calibrating the torque sensor involved taking a 10-20 second sample of data in mV at roughly every 0.2 N of force, ranging from 0 – 1.2 N. The readings over each sample were then averaged and the average sensor output vs. force applied was plotted and fit linearly, finding that $F = 343.13x + 0.3231$.

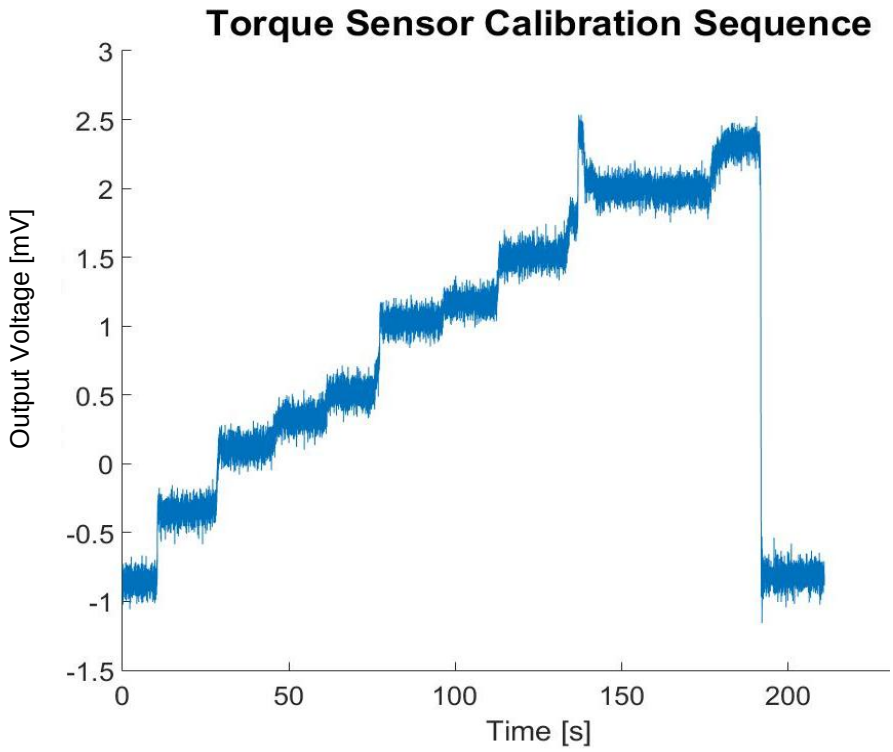

Figure 36. The calibration sequence for the torque sensor required several seconds of voltage data be collected at a recorded force applied.

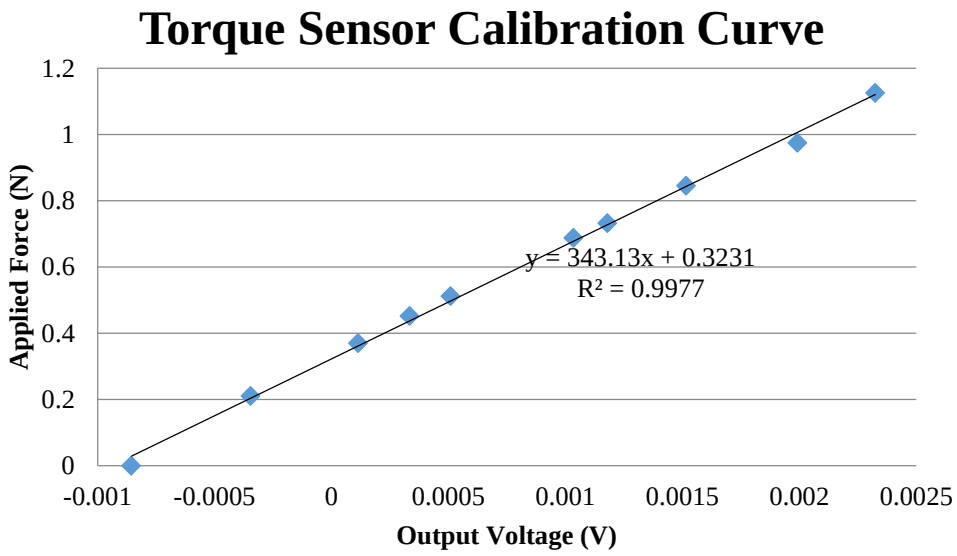

Figure 37. The values of applied force and output voltage of the torque sensor were correlated via a calibration curve.

The Setra in-line pressure sensor was calibrated using the manufacturer's calibration data. The plot of calibration points can be seen below:

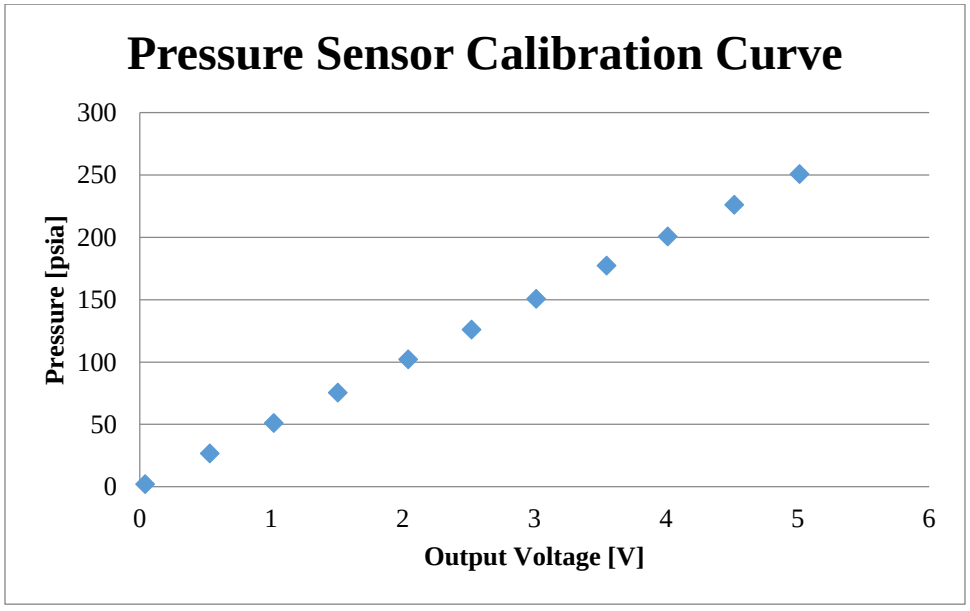

Figure 38. Manufacturer data was used to generate the calibration curve for the Setra pressure sensor.

4.1.2 Nitrogen Thrust Tests

To verify all components of the system were functioning properly, a test fire was conducted using pressurized nitrogen gas. A two way valve connecting a ¼ inch tube to the system was manually pulsed in 10 second intervals. The resulting thrust and chamber pressure were recorded in Figure 39.

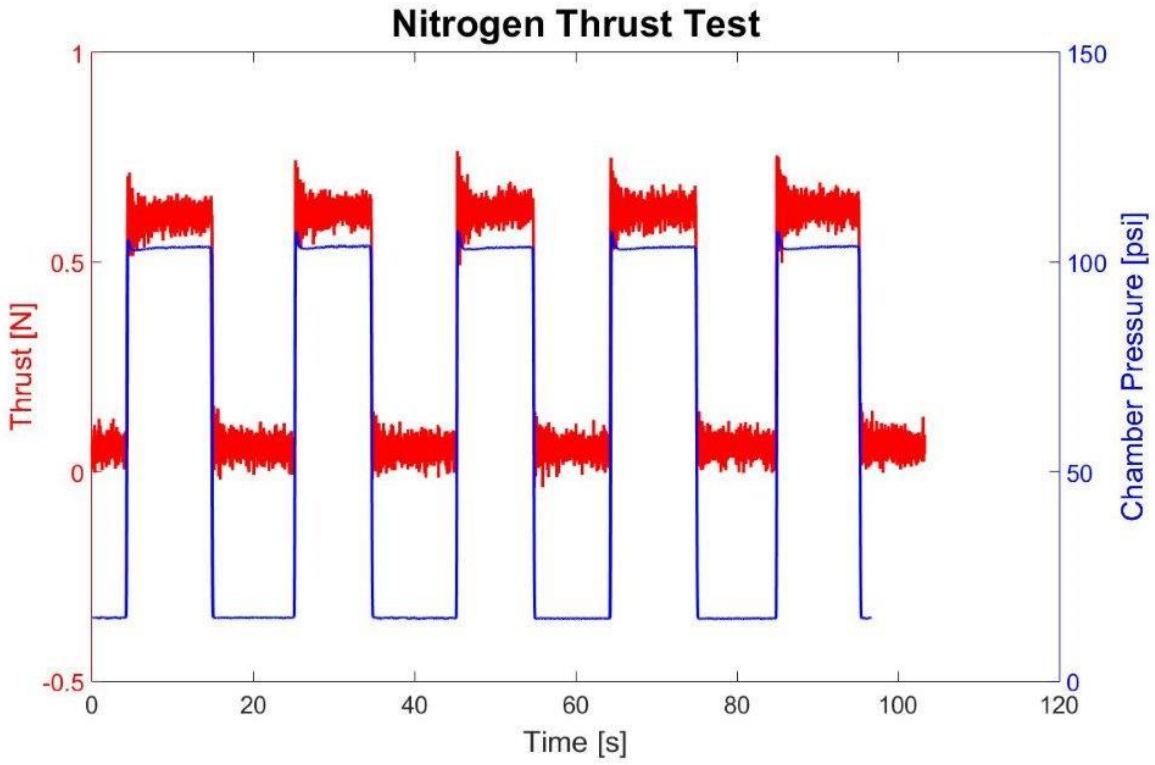

Figure 39. Test firing began with nitrogen gas to validate the system. A thrust of .6 N and chamber pressure of 100 psi was achieved, as anticipated.

Shown in blue above, the chamber pressure behaved as expected and quickly reached a value of 100 psi. Though there was a slight overshoot of the pressure initially, it settled very quickly and maintained steady at the designed pressure. The thrust, indicated in red, did not

exhibit ideal behavior due to an inherently large level of noise in the data collection system. The thrust level is relatively noisy and does not precisely align with the zero value. It did reach a value close to that expected of cold gas thruster however. For the proof of concept required in this experiment, this level of accuracy is acceptable, as it will provide an acceptable indication for what is occurring in the system. The results of from this test provided the clearance to begin prepping the system for a live hydrogen peroxide test.

4.1.3 Catalyst Bed Tests

After exposing the entire system to increasing concentrations of hydrogen peroxide, the experimental setup intended to provide empirical results on catalyst bed length was begun. The first test was conducted using the 1-cm long catalyst bed. The exhaust temperature of the catalyst bed was measured and the exhaust contents condensed and collected. Theoretically, we expected to see the spike in temperature reach a significant fraction of the adiabatic decomposition temperature of 86 weight percent hydrogen peroxide, ~800 K (526 C). The results of the experiment are shown in Figure 40.

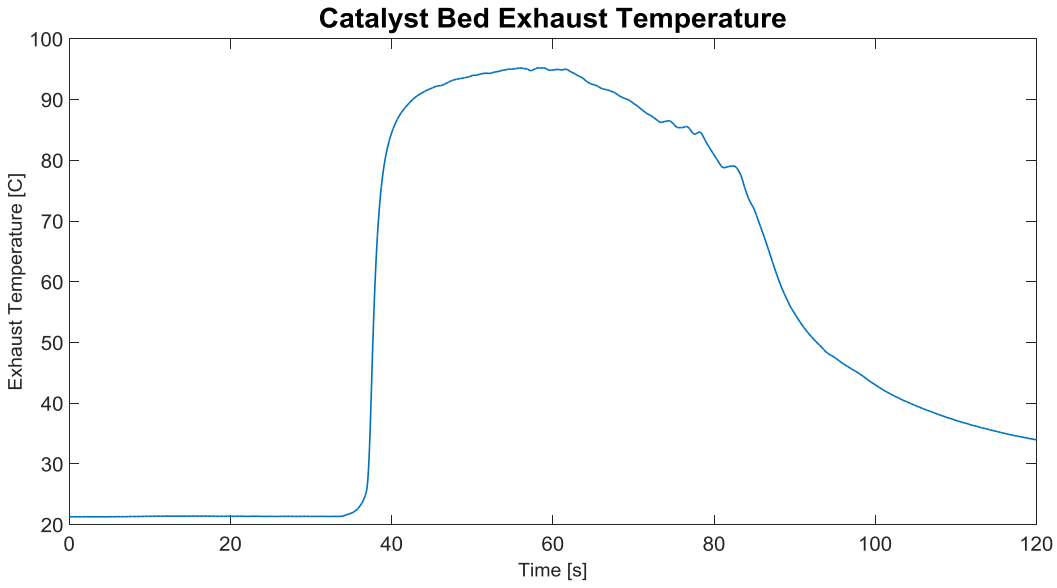

Figure 40. A test of the 1 cm long catalyst attempted to characterize percent of theoretical adiabatic decomposition temperature reached.

During the short experiment, the exhaust temperature rose immediately to 90 C and then slowly increased to 95 C before the propellant was expended and the test ended. The collected exhaust contents were then exposed to an activated catalyst bed, visually indicating a dramatically reduced concentration of peroxide.

The relatively small increase in temperature compared to the expected value was carefully considered in light of the apparent decrease in concentration of peroxide. The large thermocouple probe used in the system was determined to be a possible cause of the inaccurate temperature readings. After the bulk decomposition of hydrogen peroxide occurs in the catalyst bed, the products, specifically the water vapor, are re-condensing in the chamber and on the tip of the probe. This would cause readings of the condensation temperature of water, which is accurate with results.

Due to a constraint on the volume of peroxide secured for testing and the delay of critical components, the decision was made that the 1 cm long catalyst bed demonstrated enough

functionality to support firing the complete thruster with the 2 cm long catalyst bed it was designed to hold.

4.1.4 Hydrogen Peroxide Tests

The first test conducted with 86 weight percent hydrogen peroxide consisted of a test volume of 50 mL of peroxide and a starting feed pressure of 50 psia. The infusion rate of the pump was set at 155 mL/min which was determined experimentally with water. The results of the test can be seen in Figure 41. Just past the 50 second mark the syringe pump was activated and the Lee valve opened. It can be seen that feed pressure immediately rose to 100 psia and stayed fairly constant. The chamber pressure, temperature, and thrust curves exhibited almost identical curves. After an initial jump shortly after firing the system, these three parameters climbed linearly until the valve was shut off at 65 seconds for us to exam in the system. Presumably, this linear increase was due to the catalyst bed heating up and the reaction rate improving from the initial value. After a period of approximately 130 seconds, the valve was manually pulsed until the line was emptied. These results provide tantalizing hints at the minimum impulse bit of the system, but a better resolution sensor and experiment setup would need to be established for a realistic determination.

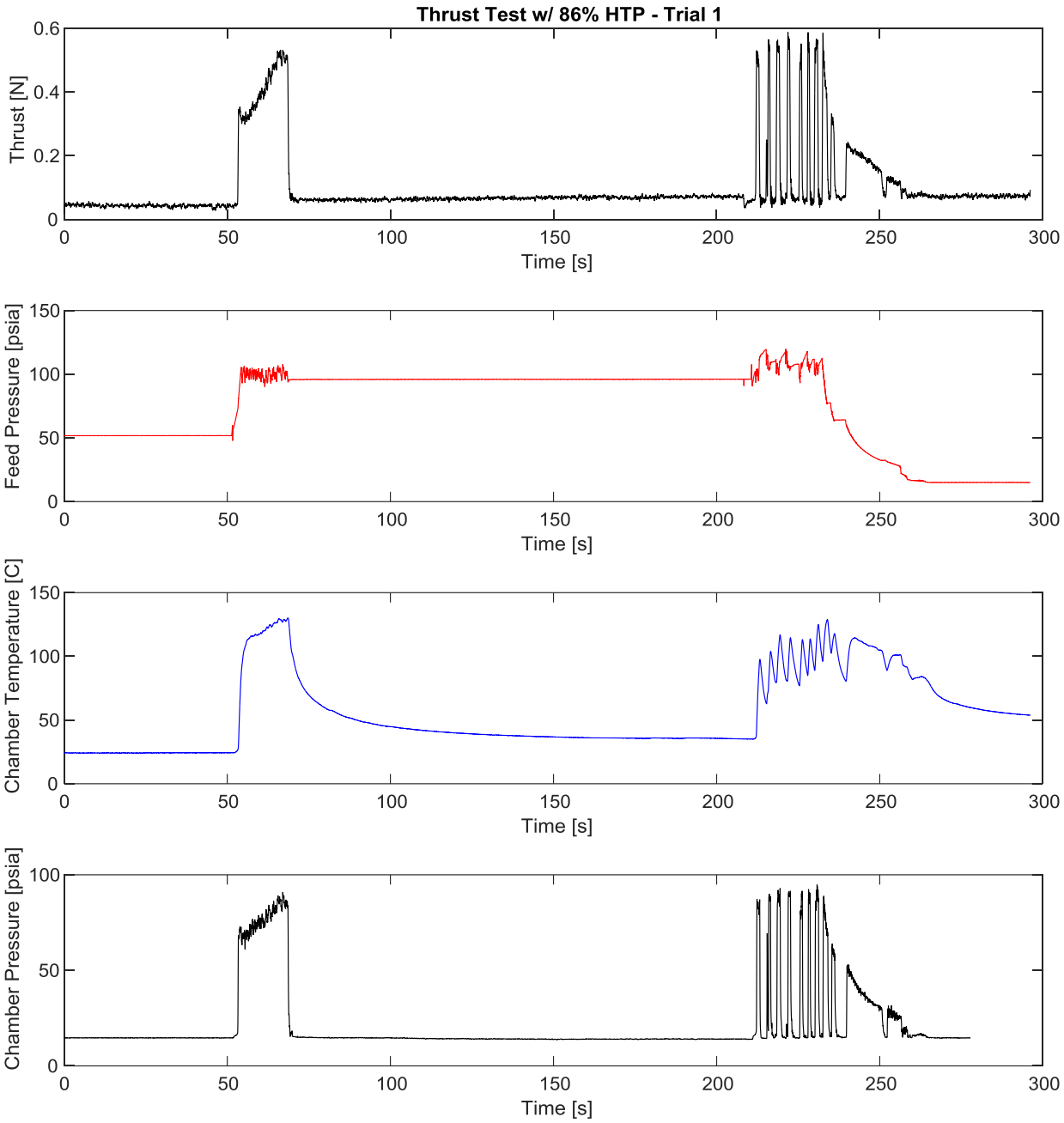

Figure 41. The first test fire consisted of two distinct sections. The valve was initially switched on at 50 seconds and performance increased as catalyst bed warmed up. The second phase was a series of manual pulses until the line was emptied. A thrust between .3 and .6 N was generated with a feed pressure of 100 psia, chamber temperature of 135 C, and chamber pressure approaching 100 psia.

It is also important to point out that a maximum thrust around .5 N was reached during the test fire. Values even closer to .6 N were achieved during the pulsing period. These values agree with those we expect to see, as this nozzle was designed to expand into a significantly lower back pressure of 7158 Pa. The temperature values rose slightly from the 95 C peak in the 1 cm catalyst bed to 135 C, supporting the theory of condensing water vapor on the thermocouple probe. The full range of catalyst experiments would need to be conducted in order to assess further. The chamber pressure approached the intended value of 100 psia, but fell slightly short at 90 psia. Overall the first firing was successful and provided a plethora of data for future analysis.

The second test firing was again 50 mL of peroxide at a starting feed pressure of 50 psia and infusion rate of 140 mL/min. The results are indicated in Figure 42. The test was allowed to run to completion after the valve was opened at 40 seconds. The feed pressure data indicates an early start on the syringe pump. The irregularities in the chamber pressure are intriguing, but not easily explainable without more competent analysis. A direct correlation between feed pressure and thrust seems to be apparent, although no other graph follows the trend precisely.

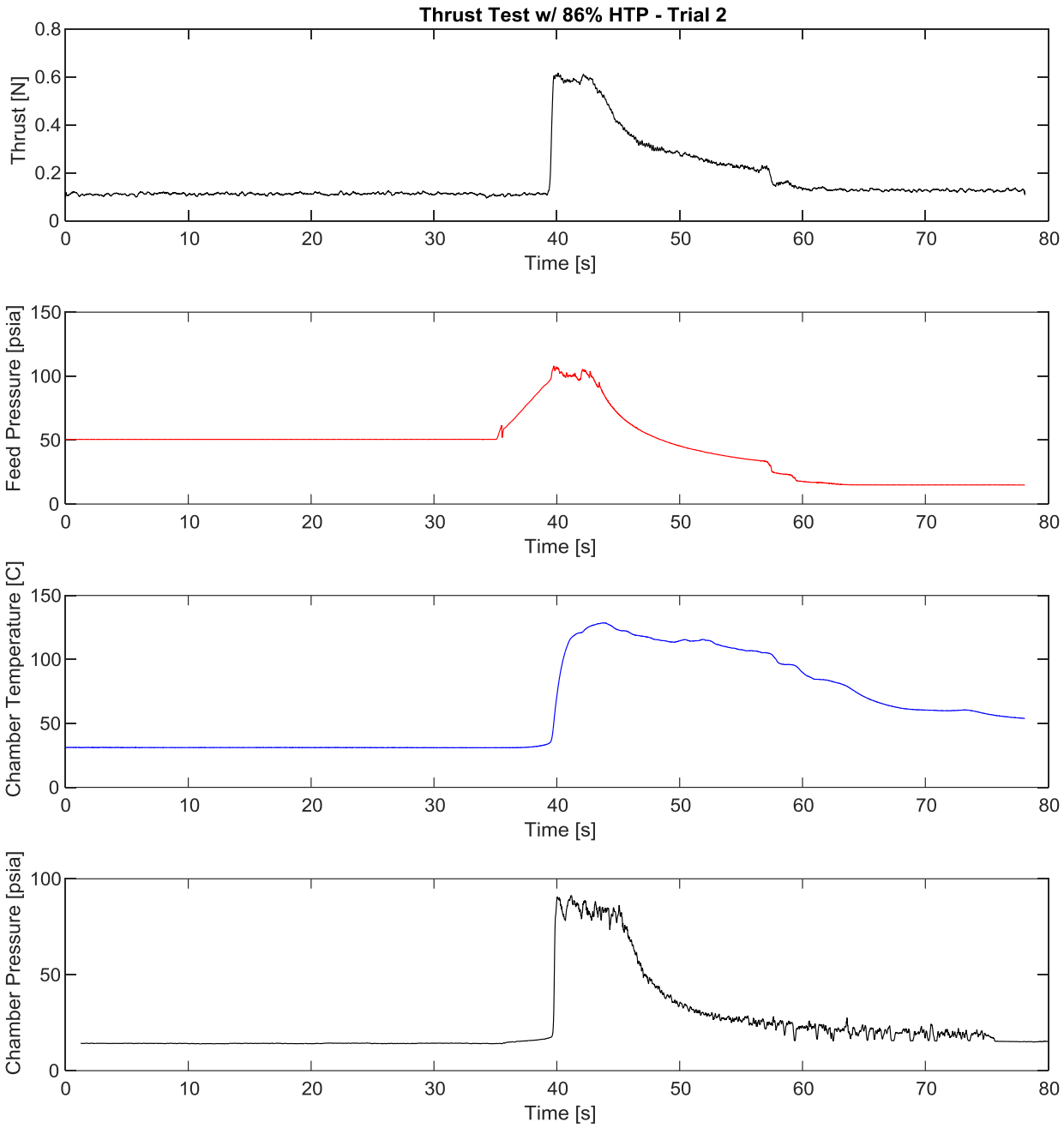

Figure 42. The second test fire began achieved similar results as Trial 1, with .5 N of thrust, a feed pressure that quickly climbed to 100 psia, a chamber temperature of 135 C, and a chamber pressure around 90 psia.

The third test fire of the system was conducted at a lower starting feed pressure of 30 psia and the same infusion rate of 140 mL/min for the syringe pump. The volume was kept constant at 50 mL. The results held consistent with Trial 1 and 2, reinforcing the prior findings. It does become apparent however, that the thrust measurements from the torque sensor are stepping away from their zero value. Though the testing began with the thrust value 'zeroed' around .05 N, it has increased to nearly .15 N by this experiment. Future work should look into obtaining a better torque sensor or recalibrating it after each test fire.

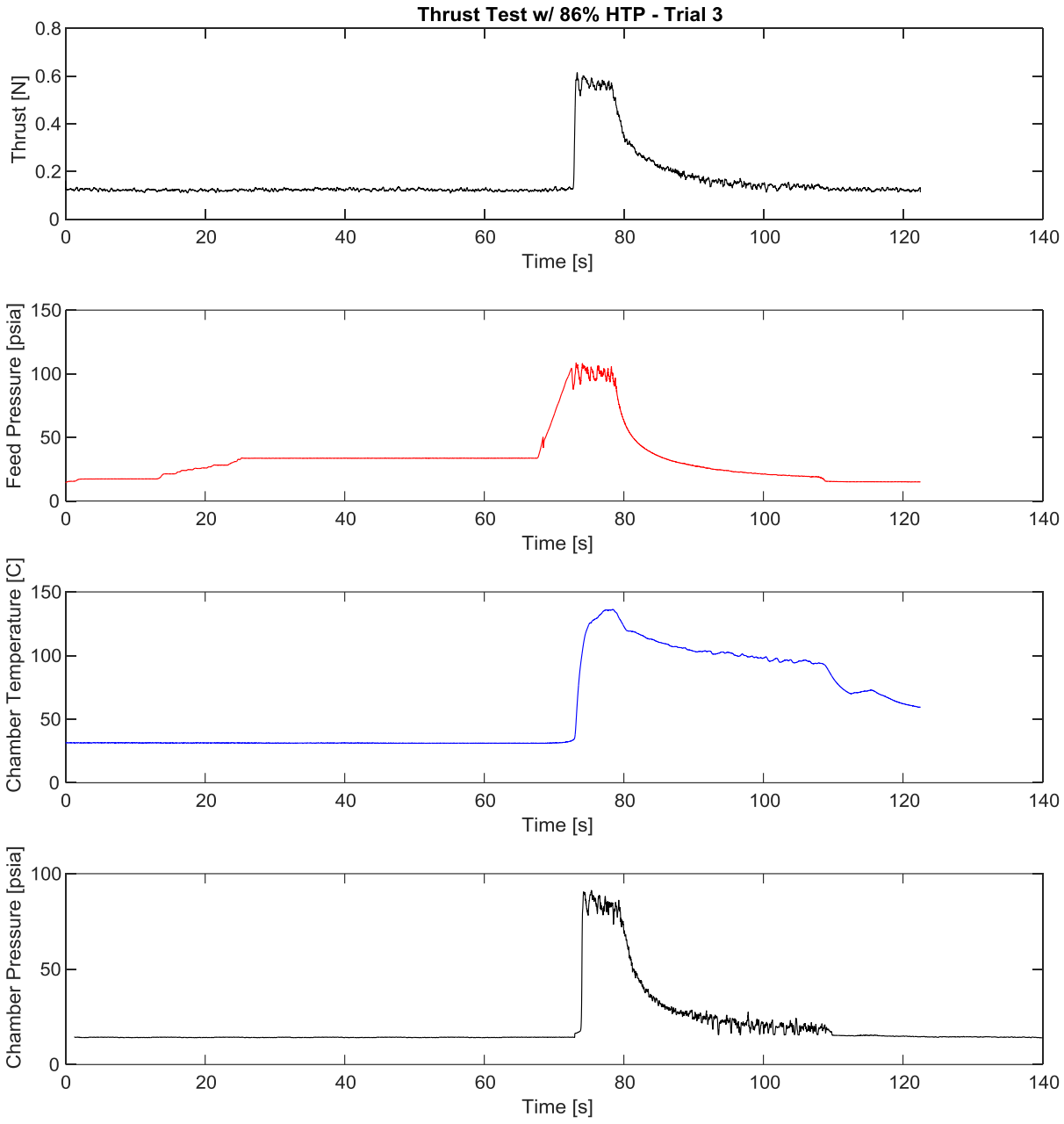

Figure 43. To begin Trial 3, the initial feed pressure was lowered to 30 psia, but quickly climbed to 100 psia once more. Similar results were obtained, but indications concerning the validity of the syringe pump as a pressurizing device arose.

The fourth trial attempted to conduct a long test fire in order to observe the systems steady state. The volume used in this experiment was 100 mL at a pump infusion rate of

140 mL/sec and starting feed pressure at 50 psia. The results varied substantially from previous test firings. The chamber pressure and thrust spiked and then immediately fell to 50 psia and .35 N, respectively. The temperature however, remained consistent with previous results.

The cause of this deviation is still unclear, though the best guess is that the increase in volume altered the functionality of the syringe pump, reducing the responsiveness and ability of the system. This, along with repeated problems in using the syringe pump, is strongly indicative that a new method for pressurizing the system needs to be identified.

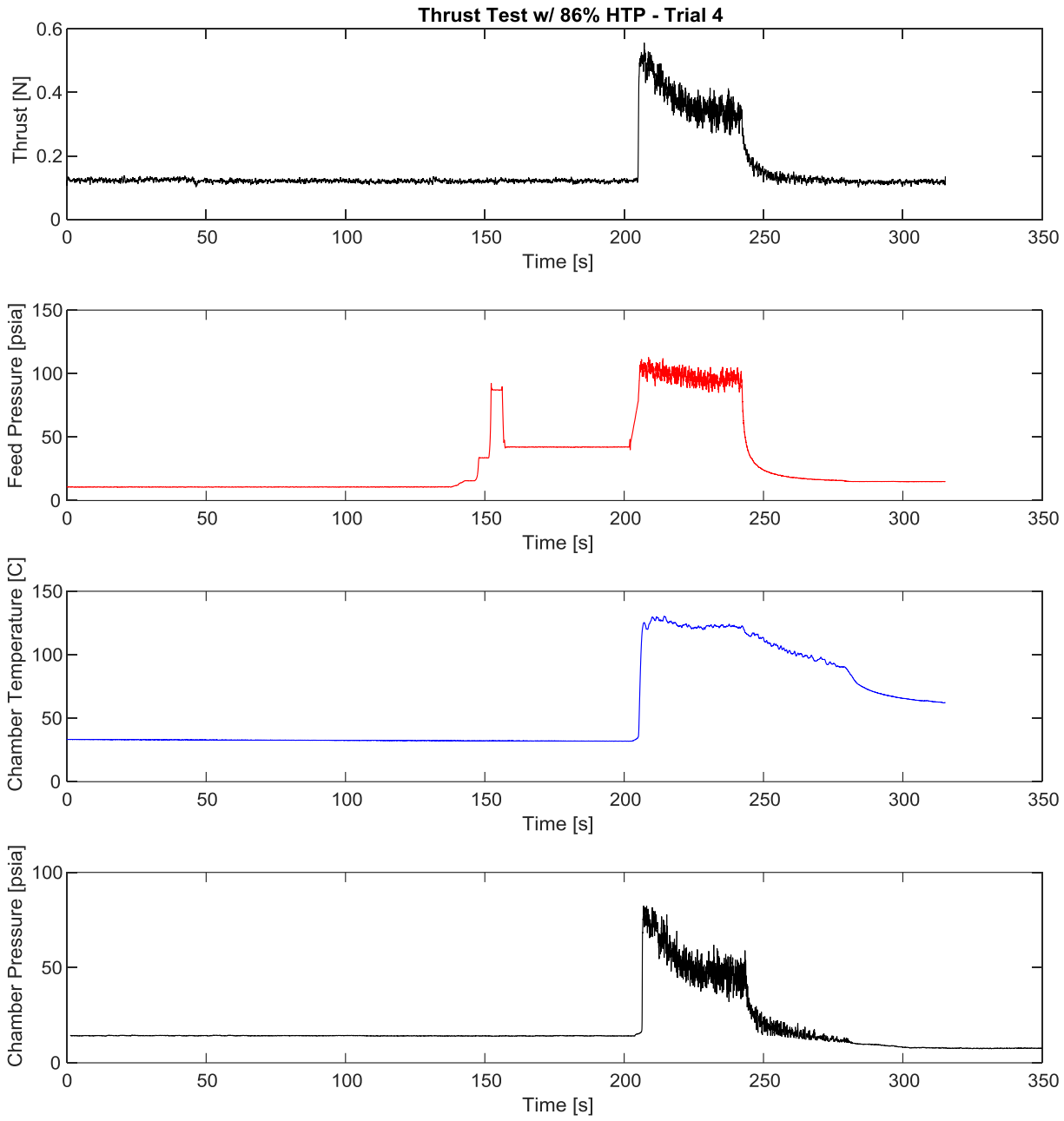

Figure 44. A final attempt at a long duration test fire resulted in a spike of expected performance, which quickly fell to a steady state at half the thrust and chamber pressure previously achieved.

5 Summary, Conclusions, and Recommendations

5.1 Summary

The increase in small satellite interests and demand on higher capabilities has prompted research into high-performance propulsion systems. This project focuses on the design and testing of a hydrogen peroxide powered propulsion system for picosatellites. After designing an objective model, a test prototype and ground support equipment, a test system was designed and built. A series of tests were conducted to determine thrust performance and hydrogen peroxide decomposition. The resulting hydrogen peroxide thruster produced the expected thrust of about 0.5 N under atmospheric conditions. These preliminary tests proved the concept; however, extensive tests with setup modifications should be conducted in the future in both atmospheric and in vacuum conditions.

5.2 Conclusions

The primary objectives, to design, build, and test a 1.25 N hydrogen peroxide thruster were successfully accomplished during the course of this MQP at MIT LL. After slight modifications, the system behaved as anticipated, providing a repeatable thrust of .5 N at sea level, and validating the conceptual design. In so doing, we have reached several important milestones in the exploration of a peroxide propulsion system for small spacecraft. Additionally, we have successfully established the ground work to serve as the strong basis towards the design and operation complete miniature propulsion system.

Some of the key results from our experiments serve as a proof of concept for various components of the setup, and provide a solid framework for continued research. Foremost we were able to demonstrate:

1. The ability of the Lab to safely store, handle, and test with high weight percent peroxide, clearing many initial hurdles concerning safety.
2. The measurement of a thrust using this propellant is possible.
3. Decomposed hydrogen peroxide can be used to pressurize an upstream chamber to the required 100 psi.
4. The design for an inexpensive, functional, and versatile catalyst bed has been identified and the geometry lends itself to our application.
5. The identification of flow control valves capable of integration into this system immediately. This should negate the need to source custom valves later at a high cost and long timeframe.

5.3 Recommendations for Future Work

Equally as important, our experiments have provided us with insight, vision, and suggestions for the improvement and progression of this project. In order of priority and timeline, they include:

- A robust and capable pressurized feed system should be implemented.
- Procure additional peroxide and continue catalyst length experiments. Special attention should be given to perfecting temperature measurements and devising a way to determine exhaust composition.
- The current system should be extensively retested in its current configuration. Focus should be on identifying specific design improvements.
- Gathering upon the knowledge gained in these tests, the thruster block and thrust stand should be redesigned for more advanced and accurate experimentation.

6 References

1. Amri R, Gibbon D, Rezoug T. The design, development and test of one newton hydrogen peroxide monopropellant thruster. Aerospace Science and Technology; 2012.
2. Ave S. Fundamentals of compressible fluid mechanics. 2006.
3. Baumgartner, H. J., et al. Decomposition of concentrated hydrogen peroxide on silver I. Low temperature reaction and kinetics. Journal of Catalysis 2.5 405-414, 1963.
4. Beutien, Trisha R., et al. Cordierite-based catalytic beds for 98% hydrogen peroxide. 10 2002.
5. Bouwmeester J, Guo J. Survey of worldwide pico-and nanosatellite missions, distributions and subsystem technology. Acta Astronautica. 2010;67(7):854-62.
6. Courtney D. Photo of Sputnik 1 1998 [Available from: http://www.rutgersprep.org/kendall/7thgrade/cycleA_2012-13/12_SP/sputnik1.html.
7. Finley K. NASA lets you build your own satellite with PhoneSat: Wired; 2012 [
8. Frieling T. The race: The uncensored story of how America beat Russia to the moon. New York, New York: Bowker Magazine Group; 1999.
9. Frost C, Agasid E, Biggs D, Conley J, Peresz AD, Faber N, et al. Small Spacecraft Technology State of the Art. Moffett Field, California: NASA Ames Research Center, 2014.
10. Gatsonis, N. A., Lu, Y., Blandino, J. J., Demetriou, M. A., and Paschalidis, N., “Micro Pulsed Plasma Thrusters for Attitude Control of a Low Earth Orbiting CubeSat”, submitted June 2015 to the AIAA Journal of Spacecraft and Rockets, in review.
11. Gibbon D, Ward J, Kay N. The design, development and testing of a propulsion system for the SNAP-1 nanosatellite. 2000.

12. Haag TW. Design of a thrust stand for high power electric propulsion devices: National Aeronautics and Space Administration; 1989.
13. Haag TW. PPT thrust stand: National Aeronautics and Space Administration; 1995.
14. Hawkins, T., Brand, A., McKay, M., & Tinnirello, M. Reduced Toxicity, High Performance Monopropellant at the U.S. Air Force Research Laboratory. Edwards AFB, CA: Air Force Research Laboratory (AFMC). 2010.
15. Helvajian H, Janson SW. Small satellites: past, present, and future: Aerospace Press; 2008.
16. Hitt D, Zhou X. One-dimensional modeling of catalyzed H2O2 decomposition in microchannel flows. AIAA Paper. 2003.
17. Klint Finley. "Nasa lets you build your own satellite with PhoneSat.". Wired. (2012-08-29). Retrieved 2013-04-25.
18. LabChem Inc. 2013. *Hydrazine Standard, 1000ppm Safety Data Sheet* [Online]. [Accessed 09/05 2015].
19. LabChem Inc. 2012. *Hydrogen Peroxide, 30% w/w Safety Data Sheet* [Online]. [Accessed 9/23/2015 2015].
20. Kuan C-K, Chen G-B, Chao Y-C. Development and Ground Tests of a 100-Millinewton Hydrogen Peroxide Monopropellant Microthruster. Journal of Propulsion and Power; 2007.
21. Mehrparvar, Arash. CubeSat Design Specification Rev. 13 (PDF). *California State Polytechnic University*. Retrieved 2014-07-07.
22. Messier D. Tiny 'Cubesats' Gaining Bigger Role in Space 2015.

23. Mueller J, Hofer R, Ziemer J. Survey of propulsion technologies applicable to cubesats; 2010.
24. Pasini A, Torre L, Romeo L, Cervone A, D'Agostino L. Testing and characterization of a hydrogen peroxide monopropellant thruster. Journal of Propulsion and Power; 2008.
25. Platt, D. A monopropellant milli-Newton thruster system for attitude control of nanosatellites. Proceedings of the 16th Annual USU Conference on Small Satellites, SSC02-VII-4; 2002
26. Rysanek F, Hartmann J, Schein J, Binder R. Microvacuum arc thruster design for a cubesat class satellite. 2002.
27. Schefter, James. *The Race: The uncensored story of how America beat Russia to the Moon*. New York: Doubleday. 1999.
28. Schumb WC, Satterfield CN, Wentworth RL. *Hydrogen Peroxide*; 1955.
29. Siddiqi AA. Sputnik and the Soviet space challenge: University Press of Florida; 2003.
30. Spanjers GG, Bromaghim DR, Lake J, White D, Schilling JH, Bushman S, et al. AFRL MicroPPT development for small spacecraft propulsion: Defense Technical Information Center; 2002.
31. Sutton GP, Biblarz O. Rocket propulsion elements: John Wiley & Sons; 2010.
32. Thomas MA, editor Design and Testing of a Hydrogen Peroxide Microelectromechanical Systems. Proceedings of the Joint AFRL/MIT Formation Flying and Micro Propulsion Workshop; 1998: George Washington University.

33. Trudel TA, Bilén SG, Micci MM, editors. Design and Performance Testing of a 1-cm Miniature Radio-Frequency Ion Thruster. Proceedings of the thirty-first international electric propulsion conference, Electric Rocket Propulsion Society, Ann Arbor, USA; 2009.
34. Ventura, M. C., et al. Advancements in high concentration hydrogen peroxide catalyst beds. AIAA/ASME/SAE/ASEE Joint Propulsion Conference and Exhibit, 37th, Salt Lake City, UT. 2001.
35. Wernimont, E., et al. Past and Present Uses of Rocket Grade Hydrogen Peroxide General Kinetics, LLC Aliso Viejo, CA. 1999.
36. Woellert K, Ehrenfreund P, Ricco AJ, Hertzfeld H. Cubesats: Cost-effective science and technology platforms for emerging and developing nations. Advances in Space Research: Elsevier; 2011. p. 663-84.

7 Appendices

Appendix A: Abbreviations and Variables

CSLI	CubeSat Launch Initiative
IGY	International Geophysical Year
COTS	Commercial Off The Shelf
MEMS	Micro-Electromechanical Systems
LEO	Low Earth Orbit
1U	One unit or One Liter
SSTL	Surrey Satellite Technologies Ltd.
ASAT	Antisatellite
MEO	Medium Earth Orbit
HEO	Highly Elliptical Orbit
GEO	Geostationary Earth Orbit
3U	Three units or Three Liters
ACS	Attitude Control System
ISISpace	Innovative Solutions in Space
SPL	Space Propulsion Laboratory at MIT
MPS	Modular Propulsion Systems
ΔV	Change in Velocity
6U	Six units or Six Liters
µPPT	micro-Pulsed Plasma Thrusters
EP	Electric Propulsion
SWaP	Size, Weight, and Power

Appendix B: Test Procedures

This document describes the steps involved in the setup and operation of a series of experiments meant to validate the concept of a hydrogen peroxide thruster. The importance of safety and emergency preparations taken in the laboratory are also addressed in detail. The following procedures and safety requirements will be followed exactly during every experiment, with the utmost attention paid to keeping the entire team safe throughout the process.

General Instructions

Complete all information required in this document while performing the test procedure. Failures should be noted explicitly at the step where the failure occurs, in addition to being summarized at the end of this document.

No excursions from this procedure are allowed in real time with high test peroxide loaded into the system. If a change to the procedure is required any hydrogen peroxide in the system must be flushed per procedure and the edits must be verified and validated using water.

Appendix C: Safety

Hydrogen Peroxide Health Hazards and First Aid

Concentrated hydrogen peroxide is corrosive to mucous membranes, eyes and skin. Prognosis of exposure depends directly on exposure duration, concentration, and location. General guidelines as to the proper action to take are detailed below by exposure type.

1. Nose and throat inhalation
    a. Result in irritation leading to coughing and difficulty in breathing.
        i. If case of repeated (or prolonged) exposure:
            1. Risk of sore throat, nose bleeds, chronic bronchitis, pulmonary edema, nausea, and vomiting.
    b. To prevent inhalation, keep head from entering fume hood.
        i. Fume hood controls inhalation risks.
    c. In the case of nose or throat inhalation, use water to wash out nose and throat.
2. Eye contact
    a. Result in eye irritation, watering, redness and swelling of eyelids, risk of serious or permanent eye lesions, and ultimately blindness.
    b. To prevent eye exposure, safety glasses and a face shield is required.
    c. In the case of eye contact, immediately utilize an eye wash to flush eyes with water.
3. Skin contact
    a. Result in pain, irritation, redness and swelling of skin, and severe burns.
    b. To prevent skin contact, using gloves, boots, and lab coats are required.
    c. In the case of skin contact, wash off immediately or use the safety shower.

4. Ingestion
    a. Fatal if swallowed, paleness/cyanosis of face, severe irritation, burns and perforation of gastrointestinal tract, as well as more corrosive effects to digestive system.
    b. To prevent ingestion, basic safety precautions must be taken by laboratory scientists to avoid placing or nearing contaminated equipment or chemicals near themselves.
    c. In case of ingestion, prompt medical attention is necessary.

Required Personnel Protective Equipment (PPE)

To minimize the risk of accidental exposure to hydrogen peroxide the following guidelines have been established for safe laboratory practices:

1. At all times in the laboratory personnel should wear:
    a. Safety glasses.
    b. Ansell PVC gloves (only when handling HTP or test equipment so to prevent contamination).
    c. DuPont Safe Spec lab coat.
2. Anytime hydrogen peroxide is to be handled, transferred, or otherwise operated with these additional items will need to be worn:
    a. Face shield
    b. Best nitrisolve gloves
    c. PVC boot covers

3. Contaminated gloves, damaged lab coats, and boot covers should be rinsed over the sink with deionized water BEFORE removal, copiously rinsed with tap water AFTER removal, allowed to dry, then disposed of in the hazardous material bin and NOT reused.
4. Contaminated face shields should be thoroughly rinsed with deionized water and allowed to dry before reuse.
5. Ansell PVC gloves should always be disposed of before leaving the lab (one time use).
6. Lab coats and boot covers should be replaced every two weeks.
7. Every item should be visually inspected before use and immediately disposed of if deemed faulty in any manner.

Test Design Safety Protocols

No individual may work with hydrogen peroxide alone in the laboratory. The total amount of hydrogen peroxide used per test has been purposely limited to less than 100 mL. Once the sample has been loaded it will be contained in a compatible, heavy duty stainless steel syringe throughout the test. The syringe will have a volumetric capacity of 200 mL to allow an ample margin of safety when handling the maximum amount of hydrogen peroxide to be fired.

A live test setup will never be stored longer than 60 minutes to reduce the probability of undesired pressure build up. To eliminate the risk of a catastrophic test failure, the pressurized line carrying hydrogen peroxide will contain a relief valve set at 100 psi greater than our expected test pressure. The hydrogen peroxide will exit the relief valve through a stainless steel muffler, substantially lowering the pressure, and enter a contained vessel of deionized water. The amount of water will be enough to dilute the entire contents of the test to 3 weight percent hydrogen peroxide with a safety factor of 1.5.

During tests using hydrogen peroxide, the fume hood will be closed and a blast shield placed over the setup. The shield will be transparent and allow for visual inspection of the test firing.

Emergency Plan

The laboratory that will be used for all experiments regarding this setup will be L-247. L-247 has been approved for the storage and use of 86 weight percent hydrogen peroxide. It is an access controlled laboratory with several emergency precautions already in place. The laboratory is equipped with a water fire extinguisher, an eye wash, and safety shower, along with a supply of water for standard and emergency dilution. The hydrogen peroxide will be stored in an approved, locked flammable material container at all times when not being transferred to a loading beaker. A supply of at least 10 L of deionized water will be stored near the hydrogen peroxide at all times.

If an emergency situation develops, the procedures listed below will be followed based upon the nature of the emergency. Both the safety and security departments will be notified of any emergency event as soon as possible.

- If an unintended reaction occurs in the fume hood, aside from during live testing, attempt to end the reaction by flooding the area with water, NOT by using the fire extinguisher. In the case of a large scale emergency close the fume hood, exit the room immediately, activate the nearest fire alarm, and exit the building. Call the Safety and Security departments immediately.

- In the event that hydrogen peroxide is spilled on an individual's personal protective equipment, it will be rinsed over the sink with deionized water BEFORE removal, copiously rinsed with tap water AFTER removal, allowed to dry, then disposed of in the hazardous material bin and NOT reused. Contaminated boot covers will be removed by another PPE clad team, turned inside out, and then washed in the sink.
- If a laboratory member is exposed to hydrogen peroxide directly, either through skin or eye contact, they will copiously rinse the affected area in the sink or eye wash. If the exposure amount is large the safety shower should be used. First aid procedures mentioned in section 1.3.1 will be followed.
- If hydrogen peroxide is spilled on any surface, it will be immediately diluted and the EHS Office consulted for clean-up.
- Every hydrogen peroxide sample will be diluted to 3 weight percent or less before being disposed of slowly with running water.
- The proper personal protective equipment guidelines, as advised in the Required PPE Section, will be followed at all times.

Passivation of Parts

The possibility of contaminants on test setup components poses a significant risk of undesirable decomposition of the hydrogen peroxide flowing through it. To prevent this, all materials will be precision cleaned per MIT Lincoln Laboratory PS-3-21 and passivated according to FMC Bulletin no. 104: Materials of Construction for use with Hydrogen Peroxide.

All wetted components will be passivated before initial use. This procedure is spelled out in *Appendix A: Abbreviations and Variables* for completeness. For as long as the system remains isolated, the passivation procedure will not be repeated. These procedures will be carried

out in an outside facility experienced in passivation. If new components are added, or the setup dismantled, the process will be repeated.

After assembling the system, all parts will be conditioned by running 35% H_2O_2 through the entire system. The 35% H_2O_2 will be supplied by PeroxyChem and will be HTP grade diluted to 35%.

Appendix D: Laboratory Protocols

Standard Lab Procedure

This procedure ensures that the laboratory is clean for usage and that personnel safety is maximized. The procedure is split into two—for entering the lab and exiting the lab. All laboratory personnel involved in our testing must perform and adhere to this procedure.

When entering the laboratory:

1. Examine personal protective equipment for damage/faults.
    a. When safety of PPE is guaranteed, don the required material.
2. Visually inspect laboratory for cleanliness.
    a. Ensure test location (fume hood, sink, etc.) is clean and fume hood is operating normally.
    b. Take measures to precision clean any unclean components involved in test setup.
3. Take notice of all other personnel in laboratory.
    a. Inform other personnel if testing is due that day.
4. Observe unobstructed escape route.
    a. If no safe escape, rearrange any obstructive objects to clear a path.

When exiting the laboratory:

1. Confirm that all chemicals have been returned to designated storage cabinet.
    a. Make sure that hydrogen peroxide storage cabinet h.as been locked.
2. Examine fume hood testing location for cleanliness
    a. Clean any test equipment that has been contaminated.
3. Removal/Disposal/Storage of PPE.
    a. Inspect PPE.
        i. If compromised dispose of it.
        ii. If deemed safe, return to PPE storage—this does not apply to PVC gloves, always dispose of PVC gloves when finished.
4. Wash hands before leaving laboratory.

Proof Testing Procedure

System Leak Test with Nitrogen Gas

The following test procedure is designed to test the system for any leaks using Nitrogen gas.

Specific Equipment Required:

- Nitrogen gas tank.
- Gas regulator (range between 0 and 500 psi).
- Completely assembled test setup with special attention that the valves A, B, C and D begin in the ‘off’ position.

1. Set up the nitrogen gas cylinder outside the fume hood, out of the way of the opening of the fume hood. Ensure it is filled and shut off.

2. Verify all two-way valves are closed and each fitting is tightly secured to its tubing.
3. Attach the nitrogen cylinder to the connector at connection point 1. Open the valve (B) to the system and slowly increase the pressure by adjusting the nitrogen regulator. Raise the pressure to 25 psi. Make note of any system changes, including visible or audible leakage.
4. If a leak is identified in the system, identify the location(s) on the operational diagram, shut off the nitrogen gas, slowly open valve (D), allowing the setup to depressurize, and thoroughly inspect the faulty components. Repair and replace as necessary. Then repeat steps 1-4.
5. Increase the pressure in 25 psi increments until the desired pressure of 150 psi is achieved. Record the system response at each increment. If a leak is identified repeat step 5.
6. Shut off the nitrogen cylinder and open valve (D) to vent the system. Then open valve (C) to add the Lee IEP Valve to the system. Repeat steps 4-6.
7. When the entire system is steady at 150 psi, apply a foaming soap and water solution to each interface, checking for remaining leakage. Identify leaks on the operational chart and disassemble for repair appropriately.
8. Shut off the nitrogen cylinder and open valve (D) to partially vent the system. When the pressure falls below 100 psi, close valve (D), and adjust the regulator to 100 psi.

Relief Valve Stress Test

This test will determine what pressure the relief valve will open at by pressurizing the system up to the set cracking pressure of the relief valve to open and reseal it.

1. Check that relief valve is secure and that Teflon tubing is attached to muffler which is in the water bucket
2. Ensure valves A and D are closed.
3. Increase regulator to 150 psi.
4. Increase regulator in 5 psi increments until the relief valve pops, waiting 10 seconds before each increase in pressure. Watch for bubbles in water bucket, and note opening pressure of relief valve. Stop regulator at a maximum of 200 psi in case the valve fails.
5. Slowly lower pressure of regulator until bubbles stop coming out of the water bucket and the relief valve reseals. Note the resealing pressure.
6. Turn off the regulator and open valve D to equalize system and atmospheric pressure.
7. Close valve D, and adjust the regulator to 150 psi. Repeat steps 3-5, noting the cracking pressure of the relief valve.

Nitrogen Gas Test

The aim of the nitrogen gas test without the catalyst bed is to test a proof of concept for our nozzle, measure thrust and to check that our sensors work.

1. Check that the nitrogen cylinder and regulator is attached firmly to valve B and that valves A and D are closed.

2. Check that all sensors are properly installed and connected to the DAQ system and laptop.
3. Pressurize the system by setting the regulator to 100 psi.
4. Arm the DAQView system.
5. Start data collection and open the Lee valve for 30 seconds. Note maximum voltage read from torque sensor. Stop data collection after the 30 seconds.
6. Repeat step 5 for 10 second, 1 second, 100 ms, 10 ms and 1 ms (if possible) pulses.
7. Depressurize the system.
8. For test with catalyst bed: Remove thrust block and add catalyst bed to thrust block. Secure thruster block back to the arm. Repeat steps 1-6 with the catalyst bed.

Appendix E: Loading the System

Chemical Loading Procedure for Liquids

The following procedure is meant to load any liquid into the test setup. To satisfy safety requirements and expose the team to a variety of practice scenarios, every liquid will be treated with the precautions afforded hydrogen peroxide. The purpose of this procedure is to keep the hydrogen peroxide isolated during the transfer process from the storage container. For the purposes of this experiment, the storage container will be a one pint storage bottle. To guarantee safety, no hydrogen peroxide sample may ever be returned to the primary storage container once it has been removed. It is important that all hydrogen peroxide storage and handling equipment be dedicated to hydrogen peroxide service, and all handling should take place exclusively within the fume hood.

Specific Equipment Required:

- 200 mL stainless steel syringe
- Nexus 6000 Syringe Pump
- 2 x 400 mL Pyrex glass beakers
- Completely assembled test setup with special attention that the valves outlined below begin in the 'off' position.

  (A) Valve used to disconnect pump from the system.

  (B) Valve used for loading hydrogen peroxide.

  (C) Valve used for main test firing.

  (D) Valve used for removing air from the system.

The process for loading the stainless steel syringe with any liquid has been outlined below:

1. Ensure there is no obstruction between the H_2O_2 storage container and the fume hood for safe transferring.
2. Make sure that the handling equipment and test stand have been precision cleaned, and that the wetted components have been passivated.
3. Place a 400 mL Pyrex beaker used for loading in the front of the fume hood, near the exit of valve B. Place a 250 mL Pyrex beaker at the exit of valve D.
4. Make sure the 316 stainless steel syringe, initially unmounted on the Nexus 6000 syringe pump but fitted to the test setup, is kept stable on the pump stand.
5. Don the appropriate H_2O_2 handling PPE. Unlock the hydrogen peroxide storage cabinet and safely transport the hydrogen peroxide container to the fume hood.

6. Carefully remove the cap from the hydrogen peroxide container and pour the desired test volume into the 400 mL Pyrex glass beaker used for loading. Recap the container and return it to the storage cabinet. Then move the hydrogen peroxide filled beaker from its pouring location to its loading location in the test setup.
7. Initially keeping all two-way valves (A), (B), (C), and (D) closed, insert the end of the Teflon soft-tube used for loading into the glass beaker full of hydrogen peroxide. Similarly, insert another end of Teflon soft-tube used for relieving air from the system into the glass beaker full of deionized water.
8. Opening two-way valves (A) and (B), pull the plunger back on the stainless steel syringe to withdraw 20 mL of hydrogen peroxide from the hydrogen peroxide filled beaker into the syringe.
9. Close two-way valve (B). Ensuring that valve (B) is closed, open valves (C) and (D). Valves (A), (C), and (D) should be open at this point.
10. Pivot the stainless steel syringe from its horizontal position on the stand to a vertical position, with the fitting facing upright. Push gently on the plunger, while observing the transparent Teflon soft-tubing located at the exit of two-way valve (D)—when the hydrogen peroxide passes into view at the exit of two-way valve (D), stop pushing on the plunger and close two-way valve (D). This step is done to remove air already present in the tubing and valves in order to avoid disturbances in the flow at startup of our test firing.
11. Close valve (C). Then open valve (B) to withdraw the remaining volume of hydrogen peroxide from the hydrogen peroxide filled beaker into the syringe. Close valve (B).

12. Pour enough deionized water into the now empty glass beaker used to load hydrogen peroxide to dilute any remnant of hydrogen peroxide at a safety factor of 1.5 to get the hydrogen peroxide weight percentage to less than 3w%. For the glass beaker filled with deionized water located under the tube where air was relieved, the amount of water already exceeds the safety requirement of diluting any hydrogen peroxide that could have dripped to 3w% however more deionized water will be added for safety reassurance.
13. Mount the stainless steel syringe into the syringe pump. Set pressure of the pump to 100 psi, but do not activate the pump.
14. Open valve (C) for full access to main firing system.
15. The test setup is now ready for next steps.

All transfer materials should then be rinsed with deionized water and allowed to air dry. They should then be stored in a clean environment until further needed.

Appendix F: Purging Procedure

The purpose of this procedure is to purge the test setup of hydrogen peroxide by running deionized water throughout the system to remove hydrogen peroxide residue. The deionized water used will be provided onsite at MIT Lincoln Laboratory. We will also use this procedure after our practice water test-fires to become proficient at the procedure.

1. Check temperature readings from thermocouple attached to the syringe to ensure it is safe to handle.
2. Turn off valve A and ensure that a second syringe filled with deionized water is securely connected to the tee immediately after the first syringe.

3. Open valve A and purge the system by pushing the 200 mL of water through the whole system.
4. After the system has cooled, remove the blast shield and fill the 400 mL beaker with deionized water.
5. Refill the water syringe by opening valve B and pulling back on the syringe handle.
6. Purge the system again by pushing the water through the system. Repeat 8-10 times.
7. Close valves A and B. Remove the 400 mL beaker and attach the nitrogen regulator to the designated fitting at (1). Set the regulator at 50 psi and run nitrogen gas through the system for 2 minutes. Repeat entire procedure as needed.

This concludes the proof testing phase of the test procedure. The next phase of testing will not start until all team members are competent and confident in the procedures above. This phase of testing includes live testing of hydrogen peroxide.

Appendix G: Checklists for Operating Hydrogen Peroxide Test Firing

Our checklists for testing hydrogen peroxide are comprehensive procedures to be followed whenever tests are to be performed. This will significantly lower the risk of any accident or unintended reaction and ensure that all data is recorded accurately. All tests will be completed IAW this procedure and initials are required before proceeding to the next step.

H_2O_2 Pre-Loading Checklist

The purpose for this checklist is to setup any and all test equipment prior to loading hydrogen peroxide to minimize the time that hydrogen peroxide is loaded in the test system.

1. Double check that handling equipment is compatible with hydrogen peroxide.
2. Check that all test equipment is precision cleaned.
3. Check that all wetted test equipment is passivated.
4. Secure all fittings, clamps, and valves
5. Install syringe and calibrate syringe pump.
6. Close all valves.
7. Place beaker in designated spot.
8. Cables covered with aluminum sheet.
    a. Run underneath fume hood.
    b. Connected to laptop properly.
9. Thermocouple and pressure sensor set up and calibrated by the computer.
10. Laptop software and DAQ system synchronized.
11. Clear lab of all external personnel.

H_2O_2Pre-Firing Checklist

The purpose for this checklist is to double check that all preparations for testing are set.

1. Check that the hydrogen peroxide storage container has been returned to the storage cabinet and locked.
2. Place blast shield onto the test setup.
3. Close fume hood.

H_2O_2 Post-Firing Checklist

The purpose for this checklist is to ensure safety in checking on how the test firing performed.

1. After the test firing has been conducted, assess fume hood for any external reactions or signs of unwarranted damage to the test setup without opening the fume hood.
2. Check laptop for data acquisition and recording.
3. Observe test setup for any post-firing reactions or sputtering. If no signs of ongoing reactions, open the fume hood.
4. Remove blast shield and inspect for any damage.
5. Disassemble the cables connected to the DAQ system from the test setup.
6. If any signs of leakage or precipitation from the exhaust, dilute as necessary with deionized water.
7. Prepare for purging with deionized water.

Appendix H: MatLab Code

98% High Test Peroxide Axial Nozzle Parameter Computations

```
%-------------------------------------------------------------------------
%                       CONSTANTS
%-------------------------------------------------------------------------
T1 = 1219;                % Inlet Temperature (K)
m0 = 1.025;                 % initial mass [kg]
P1 = 1378951.46/2;              % Inlet Pressure (Pa)
k = 1.251;                % Gamma
Ru = 8.3144621;           % Universal Gas Constant (J/mol*K)
mm = 26.48;               % Molecular Mass (kg/mol)
R = 1000*Ru/mm;           % Gas Constant (m^2/K*s^2)
Tt = T1*2/(k+1);        % Throat Temperature (K)
Mt = 1;                 % Mach at the Throat
lambda = 0.983;         % Conical Nozzle Correctional Factor

M1 = 0.05;               % Mach at the Inlet
g0 = 9.8066;            % gravitational constant (m/s^2)
deltaV = 50;            % Delta V
rho = 5.293*.6748+9.62*.3252;              % Density [kg/m^3]
mu = .6748*4.7734e-5+.3252*5.0361e-5;     % Dynamic viscosity using viscosity
of H2O and O2 [kg/m*s]


%-------------------------------------------------------------------------
%                       CALCULATIONS
%-------------------------------------------------------------------------
%AER = A2/At;
AER = 10;

%solM2 = solve(((1 / x) * (((1 + ((k - 1)/2) * x^2)) / ((k + 1) / 2)) ^((k +
1)/(2 * (k - 1)))) - AER, x)
M2 = 3.429358210619325832995846399671 8;

%Stagnation Temperature (K)
To = Tt * (1 + (k-1) * Mt^2 / 2);
%Exit Temperature (K)
T2 = To / (1 + (M2^2) * (k - 1) / 2);
%Exit Velocity (m/s)
V2 = M2 * (k * R * T2)^0.5;
%Exit Pressure (Pa)
P2 = P1 * (T2 / T1)^(k / (k-1));
%Effective Exhaust Velocity (m/s)
c = (2 * k * R * To / (k-1))^(0.5);

%Mass flow rate (kg/s)
%mdot = (P1 * At / sqrt(T1)) * sqrt((k / R) * (2 / (k + 1))^((k+1)/(k-1)))
%Inlet Velocity (m/s)
V1 = M1 * (k * R * T1)^0.5;

%Cone Angle
```

```
HalfAngle = 18;
%Length (m)
%L = ((D2 - Dt)/ 2) / tan(deg2rad(HalfAngle));
% and because of this 18 half angle, we use lambda = 0.983

%F = mdot * V2 * lambda + A2 * P2
F = 2.5/2

At = F / ((((P1 / sqrt(T1)) * sqrt((k / R) * (2 / (k + 1))^((k+1)/(k-1)))) *
V2) + (10 * P2))
A2 = At * 10
A1 = 11.72 * At
D2 = (4 * A2 / pi)^0.5
Dt = (D2^2 / AER)^0.5
D1 = (4 * A1 / pi)^0.5
L = ((D2 - Dt)/ 2) / tan(deg2rad(HalfAngle))

%Specific Impulse
Is = V2 / g0
%Mass Ratio
MR = exp(- deltaV / c)
%Propellent Mass Fraction
propmassfraction = 1 - MR
%Propellent Mass
mp = propmassfraction * m0
%Final Mass
mf = m0 - mp
%Burn Time
propdot = mp / mdot
%Total Impulse
It = F * propdot

mdot = (P1 * At / sqrt(T1)) * sqrt((k / R) * (2 / (k + 1))^((k+1)/(k-1)))

T = table(AER', mdot', A1', A2', At', ...
    D1', D2', Dt', L', ...
    M2', P2', T2', V2', ...
    'VariableNames', {'AER', 'mdot', 'A1', 'A2', 'At', 'D1', 'D2', 'Dt', 'L',
'M2', 'P2', 'T2', 'V2'})
```

Nitrogen Gas Axial Nozzle Parameter Computations

```
%-------------------------------------------------------------------------
%                        CONSTANTS
%-------------------------------------------------------------------------
T1 = 300;                 % Inlet Temperature (K)
m0 = 1.025;                  % initial mass [kg]
P1 = 1378951.46/4;              % Inlet Pressure (Pa)
k = 1.4;                 % Gamma
Ru = 8.3144621;            % Universal Gas Constant (J/mol*K)
mm = 18;                % Molecular Mass (kg/mol)
R = 1000*Ru/mm;            % Gas Constant (m^2/K*s^2)
Tt = T1*2/(k+1);         % Throat Temperature (K)
Mt = 1;                  % Mach at the Throat
lambda = 1;

M1 = 0.05;                % Mach at the Inlet
g0 = 9.8066;             % gravitational constant (m/s^2)
deltaV = 50;             % Delta V
rho = 5.293*.6748+9.62*.3252;              % Density [kg/m^3]
mu = .6748*4.7734e-5+.3252*5.0361e-5;      % Dynamic viscosity using viscosity
of H2O and O2 [kg/m*s]

A1 = 12.399e-06;
A2 = 10.58e-06;
At = 1.058e-06;
D1 = 3.9733e-03;
D2 = 3.6702e-03;
Dt = 1.1606e-03;

%-------------------------------------------------------------------------
%                        CALCULATIONS
%-------------------------------------------------------------------------
%AER = A2/At;
AER = 10;

%solM2 = solve(((1 / x) * (((1 + ((k - 1)/2) * x^2)) / ((k + 1) / 2)) ^((k +
1)/(2 * (k - 1)))) - AER, x)
M2 = 3.429358210619325832995846399671 8;

%Stagnation Temperature (K)
To = Tt * (1 + (k-1) * Mt^2 / 2);
%Exit Temperature (K)
T2 = To / (1 + (M2^2) * (k - 1) / 2);
%Exit Velocity (m/s)
V2 = M2 * (k * R * T2)^0.5;
%Exit Pressure (Pa)
P2 = P1 * (T2 / T1)^(k / (k-1));
%Effective Exhaust Velocity (m/s)
c = (2 * k * R * To / (k-1))^(0.5);
%Inlet Velocity (m/s)
V1 = M1 * (k * R * T1)^0.5;
%Cone Angle
HalfAngle = 18;
%Length
```

```
L = ((D2 - Dt)/ 2) / tan(deg2rad(HalfAngle))

%Mass Flow Rate
mdot = (P1 * At / sqrt(T1)) * sqrt((k / R) * (2 / (k + 1))^((k+1)/(k-1)))

F = ((P1 * At / sqrt(T1)) * sqrt((k / R) * ((2 / (k + 1))^((k + 1)/(k -
1))))) * (M2 * sqrt(k * R * T2)) * lambda + (P1 * ((T2 / T1)^(k / (k - 1))))
* (At * AER)
F = mdot*V2 + A2*P2

%Specific Impulse
Is = V2 / g0
%Mass Ratio
MR = exp(- deltaV / c)
%Propellent Mass Fraction
propmassfraction = 1 - MR
%Propellent Mass
mp = propmassfraction * m0
%Final Mass
mf = m0 - mp
%Burn Time
propdot = mp / mdot
%Total Impulse
It = F * propdot


T = table(AER', F', mdot', A1', A2', At', ...
    D1', D2', Dt', L', ...
    M2', P2', T2', V2', ...
    'VariableNames', {'AER', 'F', 'mdot', 'A1', 'A2', 'At', 'D1', 'D2', 'Dt',
'L', 'M2', 'P2', 'T2', 'V2'})
```

98% HTP Attitude Control System Nozzle Parameter Computations

```
%-------------------------------------------------------------------------
%                       CONSTANTS
%-------------------------------------------------------------------------
T1 = 1219;                  % Inlet Temperature (K)
m0 = 1.025;                   % initial mass [kg]
P1 = 1378951.46/2;                % Inlet Pressure (Pa)
k = 1.251;                  % Gamma
Ru = 8.3144621;             % Universal Gas Constant (J/mol*K)
mm = 26.48;                 % Molecular Mass (kg/mol)
R = 1000*Ru/mm;             % Gas Constant (m^2/K*s^2)
Tt = T1*2/(k+1);          % Throat Temperature (K)
Mt = 1;                   % Mach at the Throat
lambda = 0.983;

M1 = 0.05;                 % Mach at the Inlet
g0 = 9.8066;              % gravitational constant (m/s^2)
deltaV = 50;              % Delta V
rho = 5.293*.6748+9.62*.3252;               % Density [kg/m^3]
```

```
mu = .6748*4.7734e-5+.3252*5.0361e-5;      % Dynamic viscosity using viscosity
of H2O and O2 [kg/m*s]

%F = 0.02 %for 0.1 mm Dt @120 deg/s^2 for alpha/ ~1 deg/s omega
%F = .119 %for 0.25 mm Dt @712 deg/s^2 for alpha ~10.68 deg/s omega
%F = 0.47419 % for 0.5 mm Dt @2835 deg/s^2 for alpha ~42 deg/s omega

%--------------------------------------------------------------------------
%                        CALCULATIONS
%--------------------------------------------------------------------------
%AER = A2/At;
AER = 25;

%solM2 = solve(((1 / x) * (((1 + ((k - 1)/2) * x^2)) / ((k + 1) / 2)) ^((k +
1)/(2 * (k - 1)))) - AER, x)
M2 = 4.1589;


%Stagnation Temperature (K)
To = Tt * (1 + (k-1) * Mt^2 / 2);
%Exit Temperature (K)
T2 = To / (1 + (M2^2) * (k - 1) / 2);
%Exit Velocity (m/s)
V2 = M2 * (k * R * T2)^0.5;
%Exit Pressure (Pa)
P2 = P1 * (T2 / T1)^(k / (k-1));
%Effective Exhaust Velocity (m/s)
c = (2 * k * R * To / (k-1))^(0.5);

%Mass flow rate (kg/s)
%mdot = (P1 * At / sqrt(T1)) * sqrt((k / R) * (2 / (k + 1))^((k+1)/(k-1)))
%Inlet Velocity (m/s)
V1 = M1 * (k * R * T1)^0.5;

%Cone Angle
HalfAngle = 18;
% and because of this 18 half angle, we use lambda = 0.983

%F = mdot * V2 * lambda + A2 * P2

At = F / ((((P1 / sqrt(T1)) * sqrt((k / R) * (2 / (k + 1))^((k+1)/(k-1)))) *
V2) + (10 * P2))
A2 = At * AER
A1 = 11.72 * At
D2 = (4 * A2 / pi)^0.5
Dt = (D2^2 / AER)^0.5
D1 = (4 * A1 / pi)^0.5
L = ((D2 - Dt)/ 2) / tan(deg2rad(HalfAngle))

mdot = (P1 * At / sqrt(T1)) * sqrt((k / R) * (2 / (k + 1))^((k+1)/(k-1)))

T = table(AER', mdot', A1', A2', At', ...
    D1', D2', Dt', L', ...
    M2', P2', T2', V2', ...
```

```
    'VariableNames', {'AER', 'mdot', 'A1', 'A2', 'At', 'D1', 'D2', 'Dt', 'L',
'M2', 'P2', 'T2', 'V2'})
```

Catalyst Bed Analytical Model

```
clear all;
close all;

%Code developed by Cody Slater

%--------------------------------------------------------------------------
%
%      Thermodynamic Properties
%
%--------------------------------------------------------------------------

%--------------------------------------------------------------------------
%      Heat of Formation
%--------------------------------------------------------------------------
HoF_H2O2_l                      = -187.69;              %[kJ/mol]
HoF_H2O2_g                      = -136.31;              %[kJ/mol]
HoF_H2O_l                       = -285.83;              %[kJ/mol]
HoF_H2O_g                       = -241.83;              %[kJ/mol]
HoF_O2_g                        = 0;                    %[kJ/mol]

%--------------------------------------------------------------------------
%      Specific Heat at Constant Pressure
%--------------------------------------------------------------------------
Cp_H2O2_l                      = 89.046;                %[J/mol*K]
Cp_H2O2_g                      = 43.078;                %[J/mol*K]
Cp_H2O_l                       = 75.351;                %[J/mol*K]
Cp_H2O_g                       = 33.59;                 %[J/mol*K]
Cp_O2_g                        = 29.38;                 %[J/mol*K]

%--------------------------------------------------------------------------
%      Molar Mass
%--------------------------------------------------------------------------
M_H2O2_l                      = 34.015;                 %[g/mol]
M_H2O2_g                      = 34.015;                 %[g/mol]
M_H2O_l                       = 18.015;                 %[g/mol]
M_H2O_g                       = 18.015;                 %[g/mol]
M_O2_g                        = 31.999;                 %[g/mol]

%--------------------------------------------------------------------------
%
%      Constants
%
%--------------------------------------------------------------------------
z                           = .02;      %Weight H2O2/Weight H2O2 + H2O
mol_H2O2                    = .02;      %[mol]
mol_H2O                     = (mol_H2O2 * M_H2O2_l * z)/(18 * (1-z)); %[mol]
A                           = 8 * 10^10;    %[1/s]
E                           = 13100;     %[cal/mol]
```

```
R                          = 1.987;      %[cal/mol]
k298                       = 19.79;      %[1/sec]
k393                       = 4144.7;     %[1/sec]
k421                       = 12648.7;    %[1/sec]
P                          = 689500;     %[Pa]
R_u                        = 8314;       %[J/mol*K]
R_s                        = R/M_H2O2_l;  %[J/mol*K]

%-------------------------------------------------------------------------
%
%      Adiabatic Decomposition Temperature (1H2O2 -> 1H20 + .5O2)
%
%-------------------------------------------------------------------------
HoR_decomp_ad        = abs(1 * (HoF_H2O_g) - 1 * (HoF_H2O2_l))...
                       - mol_H2O * (HoF_H2O_g - HoF_H2O_l);
%[n*Cp]H2O(g) + [n*Cp]O2(g) - [n*Cp]H2O2(l) - Latent Heat H2O [kJ per
%decomposing mole H2O2]

Tadt      = (HoR_decomp_ad * 10^3)/(((1 + mol_H2O) * Cp_H2O_g) + (.5...
                                    * Cp_O2_g)) + 298;
                        %Heat of Reaction/([n*Cp]H2O(g) + [n*Cp]02(g)) [K]

%-------------------------------------------------------------------------
%      Stage Temperatures
%-------------------------------------------------------------------------
Ta                              = 298;                    %[K]
Tb                              = 393;                    %[K]
Tc                              = 393;                    %[K]
Td                              = 421;                    %[K]
Te                              = 421;                    %[K]
Tf                              = Tadt;                   %[K]

%-------------------------------------------------------------------------
%
%     Hydrogen Peroxide Decomposition
%
%-------------------------------------------------------------------------

%-------------------------------------------------------------------------
%      Stage I
%-------------------------------------------------------------------------
HoR_decomp             = abs(1 * (HoF_H2O_g) - 1 * (HoF_H2O2_l));
%[n*Cp]H2O(g) + [n*Cp]O2(g) - [n*Cp]H2O2(l) [kJ per decomposing mole H2O2]

x1                     = (mol_H2O * Cp_H2O_l + mol_H2O2 * Cp_H2O2_l)...
                                   * (Tb - Ta)/(HoR_decomp * 10^3);

Ca                     = mol_H2O2 * 1390 * 1000 * (1/34);

Cb                     = (mol_H2O2 - x1) * 1390 * 1000 * (1/34);

dCdt1                  = k298 * Ca;

t1                     = (Ca-Cb)/(dCdt1);
```

```
rho1                    = 1390;

v1                      = (.776 * 10^(-3))/(rho1 * (2/3)*.00635^2);

L1                      = t1*v1;

%-------------------------------------------------------------------------
%       Stage II
%-------------------------------------------------------------------------
x2                  = ((mol_H2O) * HoF_H2O_g - (mol_H2O) * HoF_H2O_l)...
                                /(HoR_decomp * 10^3 );

Cc                  = (mol_H2O2 - x1-x2) * 1390 * 1000 * (1/34);

dCdt2               = k393 * Cb;

t2                  = (Cb-Cc)/(dCdt2);

rho2                = 1390 -((Tb-Ta)/20)*25;

v2                  = (.776 * 10^(-3))/(rho2 * (2/3)*.00635^2);

L2                              = t2*v2;

%-------------------------------------------------------------------------
%       Stage III
%-------------------------------------------------------------------------
x3                  = (mol_H2O * Cp_H2O_l + mol_H2O2 * Cp_H2O2_l)...
                                * (Td - Tc)/(HoR_decomp * 10^3);

Cd                  = (mol_H2O2 - x1-x2-x3) * 1390 * 1000 * (1/34);

dCdt3               = k393 * Cc;

t3                  = (Cc-Cd)/(dCdt3);

rho3                = 1390 -((Tc-Tb)/20)*25;

v3                  = (.776 * 10^(-3))/(rho3 * (2/3)*.00635^2);

L3                  = t3*v3;

%-------------------------------------------------------------------------
%       Stage V
%-------------------------------------------------------------------------
x5       = (mol_H2O * Cp_H2O_g + (mol_H2O2 - x1 - x2 - x3) * Cp_H2O2_g)...
                                * (Tf - Te)/(HoR_decomp * 10^3);

Cf       = .00001;
Ce       = (mol_H2O2 - x1 - x2 - x3 - x5) * 1390 * 1000 * (1/34);

k5_START                        = 0;
k5_STOP                         = 10*10^8;
```

```
NUM_ELEM                          = 100;
k5                                = linspace(k5_START, k5_STOP, NUM_ELEM);
dCdt5                             = k5 .* Cf;
t5                                = (Ce-Cf)./(dCdt5);

rho5                             = 100;

v5                               = (.776 * 10^(-3))/(rho5 * (2/3)*.00635^2);

L5                               = t5.*v5;

%-------------------------------------------------------------------------
%      Stage IV
%-------------------------------------------------------------------------
x4                                = mol_H2O2 - x1 - x2 -x3 - x5;

dCdt4                             = k421 * Ce;

t4                                = (Cc - Ce)/(dCdt3);

rho4                             = 250;%approximately 20% steam

v4                               = (.776 * 10^(-3))/(rho4 * (2/3)*.00635^2);

L4                               = t4*v4;

%-------------------------------------------------------------------------
%     Time
%-------------------------------------------------------------------------
% t                                 = t1 + t2 + t3 + t4 + t5;
%
% v                                   = (.776 * 10^(-3))/(1390 * (2/3)*.00635^2);
%[m/s]
%
L                                 = L1 + L2 + L3 + L4 + L5;

%-------------------------------------------------------------------------
%     Check for mass fractions
%-------------------------------------------------------------------------
mass_fraction = (mol_H2O2*M_H2O2_l)/((mol_H2O2*M_H2O2_l)+(mol_H2O*...
    M_H2O_l));

mass_fraction_peroxide_1 = ((mol_H2O2-x1)*M_H2O2_l)/(((mol_H2O2-x1)*...
    M_H2O2_l)+((mol_H2O+x1)*M_H2O_l)+(((x1/2))*M_O2_g));
mass_fraction_water_1 = ((mol_H2O+x1)*M_H2O_l)/(((mol_H2O2-x1)*M_H2O2_l)...
    +((mol_H2O+x1)*M_H2O_l)+(((x1/2))*M_O2_g));
mass_fraction_oxygen_1 = (((x1/2))*M_O2_g)/(((mol_H2O2-x1)*M_H2O2_l)+...
    ((mol_H2O+x1)*M_H2O_l)+(((x1/2))*M_O2_g));

mass_fraction_peroxide_2 = ((mol_H2O2-x1-x2)*M_H2O2_l)/(((mol_H2O2-x1-x2)...
    *M_H2O2_l)+((mol_H2O+x1+x2)*M_H2O_l)+(((x1+x2)/2)*M_O2_g));
mass_fraction_water_2 = ((mol_H2O+x1+x2)*M_H2O_l)/(((mol_H2O2-x1-x2)*...
    M_H2O2_l)+((mol_H2O+x1+x2)*M_H2O_l)+(((x1+x2)/2)*M_O2_g));
mass_fraction_oxygen_2 = (((x1+x2)/2)*M_O2_g)/(((mol_H2O2-x1-x2)*...
```

```
    M_H2O2_l)+((mol_H2O+x1+x2)*M_H2O_l)+(((x1+x2)/2)*M_O2_g));

mass_fraction_peroxide_3 = ((mol_H2O2-x1-x2-x3)*M_H2O2_l)/...
    (((mol_H2O2-x1-x2-x3)*M_H2O2_l)+((mol_H2O+x1+x2+x3)*M_H2O_l)+...
    (((x1+x2+x3)/2)*M_O2_g));
mass_fraction_water_3 = ((mol_H2O+x1+x2+x3)*M_H2O_l)/(((mol_H2O2-x1-...
    x2-x3)*M_H2O2_l)+((mol_H2O+x1+x2+x3)*M_H2O_l)+(((x1+x2+x3)/2)*M_O2_g));
mass_fraction_oxygen_3 = (((x1+x2+x3)/2)*M_O2_g)/(((mol_H2O2-x1-x2-...
    x3)*M_H2O2_l)+((mol_H2O+x1+x2+x3)*M_H2O_l)+(((x1+x2+x3)/2)*M_O2_g));

mass_fraction_peroxide_4 = ((mol_H2O2-x1-x2-x3-x4)*M_H2O2_l)/...
    (((mol_H2O2-x1-x2-x3-x4)*M_H2O2_l)+((mol_H2O+x1+x2+x3+x4)*M_H2O_l)...
    +(((x1+x2+x3+x4)/2)*M_O2_g));
mass_fraction_water_4 = ((mol_H2O+x1+x2+x3+x4)*M_H2O_l)/(((mol_H2O2-...
    x1-x2-x3-x4)*M_H2O2_l)+((mol_H2O+x1+x2+x3+x4)*M_H2O_l)+(((x1+x2+...
    x3+x4)/2)*M_O2_g));
mass_fraction_oxygen_4 = (((x1+x2+x3+x4)/2)*M_O2_g)/(((mol_H2O2-x1-...
    x2-x3-x4)*M_H2O2_l)+((mol_H2O+x1+x2+x3+x4)*M_H2O_l)+(((x1+x2+x3+x4)...
    /2)*M_O2_g));

mass_fraction_peroxide_5 = ((mol_H2O2-x1-x2-x3-x4-x5)*M_H2O2_l)/...
    (((mol_H2O2-x1-x2-x3-x4-x5)*M_H2O2_l)+((mol_H2O+x1+x2+x3+x4+x5)*...
    M_H2O_l)+(((x1+x2+x3+x4+x5)/2)*M_O2_g));
mass_fraction_water_5 = ((mol_H2O+x1+x2+x3+x4+x5)*M_H2O_l)/(((mol_H2O2...
    -x1-x2-x3-x4-x5)*M_H2O2_l)+((mol_H2O+x1+x2+x3+x4+x5)*M_H2O_l)+...
    (((x1+x2+x3+x4+x5)/2)*M_O2_g));
mass_fraction_oxygen_5 = (((x1+x2+x3+x4+x5)/2)*M_O2_g)/(((mol_H2O2-...
    x1-x2-x3-x4-x5)*M_H2O2_l)+((mol_H2O+x1+x2+x3+x4+x5)*M_H2O_l)+...
    (((x1+x2+x3+x4+x5)/2)*M_O2_g));

%-------------------------------------------------------------------------
%   Plots
%-------------------------------------------------------------------------

plot(k5, L, 'g', 'LineWidth', 2);
xlabel('Reaction Rate (Stage V) [1/sec]');
ylabel('Length [m]');
title('Length vs. Reaction Rate (Stage V)');
ylim([0 .25]);
```

Appendix I: Drawings